

Stardust-NExT, Deep Impact, and the accelerating spin of 9P/Tempel 1

Michael J.S. Belton^{a,*}, Karen J. Meech^b, Steven Chesley^c, Jana Pittichová^b, Brian Carcich^d, Michal Drahus^e, Alan Harris^f, Stephen Gillam^c, Joseph Veverka^d, Nicholas Mastrodemos^c, William Owen^c, Michael F. A'Hearn^g, S. Bagnulo^h, J. Baiⁱ, L. Barrera^j, Fabienne Bastien^g, James M. Bauer^c, J. Bedient^k, B.C. Bhatt^l, Hermann Boehnhardt^m, N. Broschⁿ, Marc Buie^o, Pablo Candia^p, W.-P. Chen^q, P. Chiang^q, Young-Jun Choi^r, A. Cochran^s, Christopher J. Crockett^g, S. Duddy^t, Tony Farnham^g, Yan R. Fernández^u, Pedro Gutiérrez^v, Olivier R. Hainaut^w, Donald Hampton^x, Kimberly A. Herrmann^y, Henry Hsieh^b, M.A. Kadooka^b, H. Kaluna^b, J. Keane^b, M.-J. Kim^z, Kenneth Klaasen^c, J. Kley^b, Kevin Krisciunas^{aa}, Luisa M. Lara^v, Tod R. Lauer^{ab}, Jian-Yang Li^g, Javier Licandro^{ac,ad}, Carey M. Lisse^{ae}, Stephen C. Lowry^t, Lucy McFadden^{af}, N. Moskovitz^{ag}, Beatrice Mueller^{ah}, D. Polishookⁿ, N.S. Raja^b, T. Riesen^b, D.K. Sahu^l, Nalin Samarasinha^{ah}, G. Sarid^b, Tomohiko Sekiguchi^{ai}, S. Sonnett^b, Nicholas B. Suntzeff^{aa}, Brian W. Taylor^{y,aj}, Peter Thomas^d, Gian Paolo Tozzi^{ak}, R. Vasundhara^l, J.-B. Vincent^m, Lawrence H. Wasserman^y, Bryant Webster-Schultz^{al}, B. Yang^b, T. Zenn^b, H. Zhao^{am}

^a Belton Space Exploration Initiatives, LLC, 430 S. Randolph Way, Tucson, AZ 85716, USA

^b Institute for Astronomy, University of Hawaii, Honolulu, HI 96822, USA

^c Jet Propulsion Laboratory, 4800 Oak Grove Dr., Pasadena, CA 91109, USA

^d Center for Radiophysics and Space Research, Cornell University, Ithaca, NY 14853, USA

^e Department of Earth and Space Sciences, University of California, Los Angeles, CA 90095, USA

^f Space Science Institute, 4750 Walnut Street, Suite 205, Boulder, CO 80301, USA

^g Department of Astronomy, University of Maryland, College Park, MD 20742, USA

^h Armagh Observatory, College Hill, Armagh BT61 9DG, United Kingdom

ⁱ Yunnan Astronomical Observatory, Chinese Academy of Sciences, P.O. Box 110, Kunming 65011, Yunnan, PR China

^j Universidad Metropolitana de Ciencias de la Educación, Dep. Física, Avda. Jose Pedro Alessandri 774, Santiago, Chile

^k University of Hawaii, Honolulu, HI 96822, USA

^l Indian Institute of Astrophysics, II Block, Koramangala, Bangalore 560 034, India

^m Max-Planck Institut für Sonnensystemforschung, Max-Planck Str. 2, 37191 Katlenburg-Lindau, Germany

ⁿ Dept. Geophysics and Planetary Sciences, Tel Aviv University, 69978 Te-Aviv, Israel

^o Southwest Research Institute, 1050 Walnut St., Suite 300, Boulder, CO 80302, USA

^p Gemini Observatory, c/o AURA, casilla 603, La Serena, Chile

^q Grad. Inst. Of Astronomy, National Central Univ., 300 Jhongda Road, Jhongli 32001, Taiwan

^r Korea Astronomy and Space Science Institute, 776 Daedukdaero, Yuseong-gu, Daejeon 305-348, South Korea

^s Univ. Texas, Dept. of Astronomy, 1 University Station, C1400, Austin, TX 78712, USA

^t Centre for Astrophysics and Planetary Science School of Physical Sciences, University of Kent, Canterbury CT2 7NH, UK

^u Department of Physics, University of Central Florida, 4000 Central Florida Blvd., Orlando, FL 32816-2385, USA

^v Instituto de Astrofísica de Andalucía – CSIC, Box 3004, E-18080 Granada, Spain

^w European Southern Observatory, Casilla 19001, Santiago 19, Chile

^x Geophysical Institute, Univ. AK, 903 Koyukuk Dr., Fairbanks, AK 99775-7320, USA

^y Lowell Observatory, 1400 Mars Hill Rd., Flagstaff, AZ 86001, USA

^z Department of Astronomy, College of Science, 134 Sinchon-dong, Sodaemun-gu, Seoul 120-749, South Korea

^{aa} Texas A&M University, Department of Physics, College Station, TX 77843, USA

^{ab} National Optical Astronomy Observatory, 950 N. Cherry Ave., Tucson, AZ 85719, USA

^{ac} Instituto de Astrofísica de Canarias, Via Lactea, 38200 La Laguna, Tenerife, Spain

^{ad} Departamento de Astrofísica, Universidad de la laguna, E-38205 La Laguna, Tenerife, Spain

^{ae} Planetary Exploration Group, Space Department, Johns Hopkins University Applied Physics Laboratory, 11100 Johns Hopkins Rd., Laurel, MD 20723, USA

^{af} NASA/Goddard Space Flight Center, Greenbelt, MD 20771, USA

^{ag} Dept. of Terrestrial Magnetism, Carnegie Institution of Washington, Washington, DC 20015, USA

^{ah} Planetary Science Institute, 1700 E. Ft. Lowell Rd., #106, Tucson, AZ 85719-2395, USA

^{ai} National Astronomical Observatory, 2-21-1, Osawa, Mitaka, Tokyo 181-8588, Japan

^{aj} Institute for Astrophysical Research, Boston University, 725 Commonwealth Avenue, Boston, MA 02215, USA

^{ak} INAF Osservatorio Astrofisico di Arcetri, Firenze, I-50125, Italy

^{al} HAS, 47-728 Hui Kelu St. #9, Kaneohe, HI 96744, USA

^{am} Purple Mountain Obs. Chinese Academy of Sciences, 2# West Beijing Road, Nanjing 210008, PR China

* Corresponding author. Fax: +1 520 795 6220.

E-mail address: mbelton@dakotacom.net (M.J.S. Belton).

ARTICLE INFO

Article history:

Available online 13 January 2011

Keywords:

Comets
Comets, Nucleus
Rotational dynamics
Comet Tempel 1

ABSTRACT

The evolution of the spin rate of Comet 9P/Tempel 1 through two perihelion passages (in 2000 and 2005) is determined from 1922 Earth-based observations taken over a period of 13 year as part of a World-Wide observing campaign and from 2888 observations taken over a period of 50 days from the Deep Impact spacecraft. We determine the following sidereal spin rates (periods): $209.023 \pm 0.025^\circ/\text{dy}$ (41.335 ± 0.005 h) prior to the 2000 perihelion passage, $210.448 \pm 0.016^\circ/\text{dy}$ (41.055 ± 0.003 h) for the interval between the 2000 and 2005 perihelion passages, $211.856 \pm 0.030^\circ/\text{dy}$ (40.783 ± 0.006 h) from Deep Impact photometry just prior to the 2005 perihelion passage, and $211.625 \pm 0.012^\circ/\text{dy}$ (40.827 ± 0.002 h) in the interval 2006–2010 following the 2005 perihelion passage. The period decreased by 16.8 ± 0.3 min during the 2000 passage and by 13.7 ± 0.2 min during the 2005 passage suggesting a secular decrease in the net torque. The change in spin rate is asymmetric with respect to perihelion with the maximum net torque being applied on approach to perihelion. The Deep Impact data alone show that the spin rate was increasing at a rate of $0.024 \pm 0.003^\circ/\text{dy}/\text{dy}$ at JD2453530.60510 (i.e., 25.134 dy before impact), which provides independent confirmation of the change seen in the Earth-based observations.

The rotational phase of the nucleus at times before and after each perihelion and at the *Deep Impact* encounter is estimated based on the Thomas et al. (Thomas et al. [2007], *Icarus* 187, 4–15) pole and longitude system. The possibility of a 180° error in the rotational phase is assessed and found to be significant. Analytical and physical modeling of the behavior of the spin rate through of each perihelion is presented and used as a basis to predict the rotational state of the nucleus at the time of the nominal (i.e., prior to February 2010) *Stardust-NExT* encounter on 11 February 2011 February 14 at 20:42.

We find that a net torque in the range of $0.3\text{--}2.5 \times 10^7$ kg m² s⁻² acts on the nucleus during perihelion passage. The spin rate initially slows down on approach to perihelion and then passes through a minimum. It then accelerates rapidly as it passes through perihelion eventually reaching a maximum post-perihelion. It then decreases to a stable value as the nucleus moves away from the Sun. We find that the pole direction is unlikely to precess by more than $\sim 1^\circ$ per perihelion passage. The trend of the period with time and the fact that the modeled peak torque occurs before perihelion are in agreement with published accounts of trends in water production rate and suggests that widespread H₂O out-gassing from the surface is largely responsible for the observed spin-up.

© 2011 Elsevier Inc. All rights reserved.

1. Introduction

In their assessment of the spin state of Comet 9P/Tempel 1 following the *Deep Impact* encounter A'Hearn et al. (2005) found a sidereal period of 1.701 ± 0.014 dy (40.82 h; $211.6 \pm 1.7^\circ/\text{dy}$). Thomas et al. (2007) determined the sense of spin to be direct and the preliminary pole position was RA = 5° , Dec = $+78^\circ$ ($\pm 10^\circ$ on the sky) roughly 11° from one of the two, photometrically degenerate, i.e. photometrically, but not geometrically, equivalent, directions (46° , $+73^\circ$) found earlier by Belton et al. (2005a) using ground-based photometry. A'Hearn et al. (2005) also noted that the pre-impact rotation period of 1.744 ± 0.006 dy (41.86 h; $206.42^\circ/\text{dy}$) determined by Belton et al. (2005a) differed significantly from the *Deep Impact* value and suggested that the difference might be explained by an inadvertent shift in the analysis of Earth-based data by a half or whole cycle between observing runs. Later, Belton et al. (2006) improved the *Deep Impact* sidereal period estimate to 1.6976 ± 0.0096 dy (40.74 h; $212.06 \pm 1.2^\circ/\text{dy}$) and Thomas et al. (2007) revised the pole position (J2000) to RA = 294° , Dec = 73° ($\pm 5^\circ$ on the sky). Thomas et al. also set the prime meridian as $W(t) = 252.63^\circ + 212.064^\circ d$, where d is the number of days since the standard epoch (JD 2451545.0). The chosen prime meridian passed through a 350 m, unnamed, crater just west of the impact site (Thomas et al., 2007). $W(t)$ is the angle between the chosen prime meridian and the intersection of the body equator and the standard Earth equator and defines the rotational phase of the nucleus at time t . This latter formula assumes a constant rotation period of 1.6976 dy between the time of impact (JD 2453555.73928) and the standard epoch.

The small difference between the pre-impact rotation rate and the spacecraft value would have been of little concern had it not been for the recognition by J. Veverka and his colleagues that the *Stardust* spacecraft, which had recently encountered Comet 81P/

Wild 2 (Brownlee et al., 2004), and was hibernating in deep space, could be revived, and had enough propulsion capability to reach 9P/Tempel 1 for an encounter on 11 February 14. This mission, now called *Stardust-NExT*, was selected as a *Discovery* mission of opportunity by NASA (www.astro.cornell.edu/next/Science.htm). A Level 1 science requirement of this mission is to “Image 25% of the surface previously observed in the *Deep Impact* mission at better than 80 m/pixel” in order to look for changes in the condition of the surface that might have occurred during the perihelion passage (2011 January 12.2) previous to the encounter. A secondary science goal is to image the, as yet unseen, artificial feature formed during the *Deep Impact* mission that is located at $350^\circ.W, -29^\circ.1$. This was designated as a secondary goal because, even if it were not attained, the part of the surface imaged could, especially if it were previously unseen by *Deep Impact*, lead to new insights for cometary science. To ensure that these objectives can be met, a high-precision rotational ephemeris and an assessment of its stability is required and it is for this reason that the present study was initiated.

In subsequent preparations for the *Stardust-NExT* mission it was noted that the *Deep Impact* rotation rate calculated by Belton et al. (2006) did not correctly phase the light curves obtained some 14 months earlier from the *Hubble* and *Spitzer* Space telescopes (Lamy et al., 2007; Lisse et al., 2005). This was the first quantitative indication that Comet 9P's rotation might be changing as it approached perihelion.

The theoretical basis for short timescale changes in cometary spin has been emphasized by Jewitt (1997; also summarized in Jewitt, 2004; see also Samarasinha et al., 2004) and exploratory calculations of excitation timescales have been carried out by Gutiérrez et al. (2002), Jorda and Gutiérrez (2002), and Gutiérrez and Davidsson (2007). For a small (effective radius = 3.0 ± 0.1 km; Thomas et al., 2007), underdense (bulk density ~ 400 kg m⁻³; Richard-

son et al., 2007) nucleus with a water production rate of 6×10^{27} molecules/s at the 2005 epoch (Schleicher et al., 2006) the timescale for substantial changes in the spin state is ~ 90 year based on Jewitt's formulation of spin-up time and his conjecture that the typical dimensionless moment arm for torques is ~ 0.05 . Thus, from a theoretical point of view it should not be surprising if 9P/Tempel 1 was changing its current period by $\sim 1\%$ (0.4 h) in a single perihelion pass or if the direction of the rotation pole drifted by a degree or two.

There is also a growing observational base to support the measurable presence of this effect in comets. Drahus and Waniak (2006) have shown through the introduction of a novel photometric time-series analysis technique that the rotation rate of the distant Comet C/2001 K5 (LINEAR) was perceptibly spinning-down as it receded from perihelion passage. In addition, earlier studies have found evidence of possible changes in spin rate in Comets 10P/Tempel 2 and 6P/d'Arrest (Mueller and Ferrin, 1996; Gutiérrez et al., 2003). Other evidence of the action of rotational torques includes the cases of Comets 1P/Halley, 2P/Encke and 29P/Schwassmann-Wachmann 1 each of which has been found to be in rotationally excited states (Belton et al., 1991 and references therein; Samarasinha and A'Hearn, 1991; Meech et al., 1993; Belton et al., 2005b).

Deep Impact photometry and imaging data from the ongoing worldwide Earth-based campaign on 9P/Tempel 1 (Meech et al., 2005, 2011, in press) plus an early *Hubble Space Telescope* study by Lamy et al. (2001) provide an unprecedented set of data with which to investigate the stability of the spin state of 9P/Tempel 1. The data that we use from ground-based and *HST* sources are de-

scribed in Section 2 where we separate them into three groups: Region A (1997–1999), Region B (2001–2004) and Region C (2006–2010). This grouping allows us to document the changes that occurred during the 2000 and 2005 perihelion passages. In Section 3 we present the *Deep Impact* approach photometry that we use to obtain direct evidence for an acceleration of the spin rate. In Section 4 we provide the theoretical basis and assumptions used in the analysis of the data. In Section 5 we outline the rotational analysis and present the basic results on the spin rate of the nucleus and its rotational phase. In Section 6 we discuss the dynamical evolution of the comet's spin state and construct analytical models for its changes through perihelion passage. In Section 7, we provide a general discussion of the relationship of our results with previously published studies of the comet's H₂O production rate. We also use our results to predict the rotation state we expect will be experienced by the *Stardust-NExT* mission at its encounter with 9P/Tempel 1 on 14 February, 2011. Section 8 contains a summary of our primary conclusions.

2. Earth-based observations and two independent methods of analysis

In an accompanying paper, Meech et al. (2011, in press) provide a detailed description of the *Deep Impact* and *Stardust-NExT* international observing campaign, its goals, participant contributions, observations and results. In Fig. 1 we show $R(1,1,\alpha)$ magnitudes for the entire data set after reduction to unit heliocentric and geocentric distance and where α is the solar phase angle. The rise and fall of the coma brightness around perihelion dominates the figure

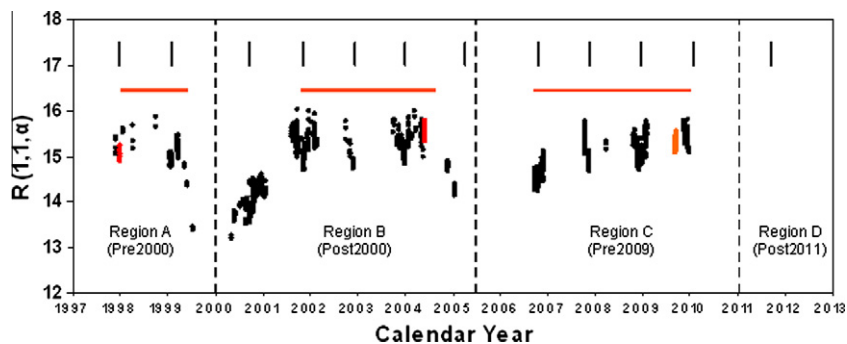


Fig. 1. 9P/Tempel 1 $R(1,1,\alpha)$ magnitudes for 1997 through 2010 from the data of Meech et al. (2011, in press, black circles) and Lamy et al. (2001, 2007, red circles). The data set contains a subset of published V magnitudes that have been converted to R using $(V-R) = 0.50$ (Li et al., 2007). The short black vertical lines show the times of opposition and the dashed vertical lines denote the time of perihelion passage. The horizontal red bars show the range of data in each region that is used in the rotational analysis. Note how the comet brightens as the solar phase angle decreases near opposition.

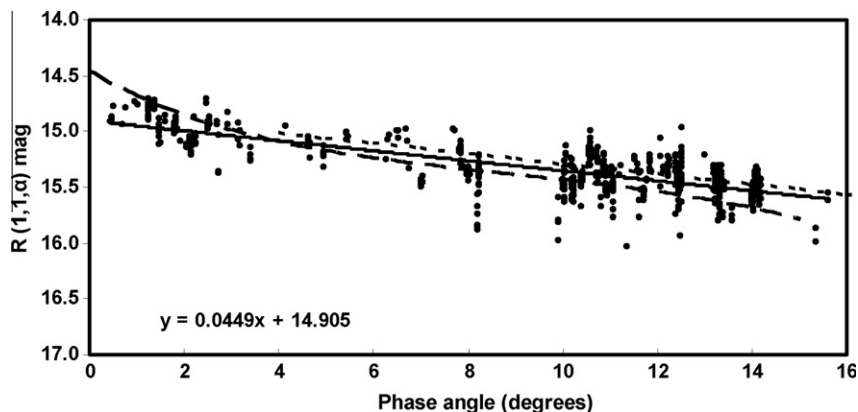


Fig. 2. Phase laws. The $R(1,1,\alpha)$ data (black dots) with various phase functions proposed for 9P/Tempel 1. Shown are the integrated phase function of Li et al. (2007) (dotted line), the phase law polynomial of Belton et al. (2005a,b) (dashed line), and a linear correlation to the data (continuous line). We use the latter ($R(1,1,\alpha) = 14.905 + 0.045\alpha$) to correct the magnitudes to zero phase angle (α).

and the substantial effect of diminishing solar phase angle at the oppositions of 2000, 2002, 2003, 2004, 2006, 2008 and 2010 is clear. A small subset of these data was obtained as V magnitudes and these have been converted to R magnitudes using $(V-R) = 0.50$ mag (Li et al., 2007). Embedded in this data set are the results of three studies done with the *Hubble Space Telescope* (HST). These were obtained in 1997 (Lamy et al., 2001), 2004 (Lamy et al., 2007) and 2009 (Meech et al., 2011, in press). The latter two were done at the request of the *Deep Impact* team in order to obtain data of sufficient quality to distinguish between alias periodicities and to measure, with the highest possible accuracy, the rotational phase of the nucleus at each epoch. The $V(1,1,\alpha)$ magnitudes in Lamy et al. (2007) were converted to $R(1,1,\alpha)$ as noted above.

All of the above photometric reductions depend on orbital information obtained from the JPL Horizons site (<http://ssd.jpl.nasa.gov/?horizons>) using the default orbit solution (K054/15) for 9P/Tempel 1. The complete set of reduced ground-based data, relevant geometry, and the timing used in this paper is listed in a supplementary electronic data file appended to Meech et al. (2011, in press). In our analysis we divided the data into three intervals each of which was expected to yield significantly different values for the spin rate: Region A, before the year 2000 perihelion passage; Region B, between the 2000 and 2005 perihelion passages; and Region C, post the 2005 perihelion passage. A fourth Region D was reserved to cover the time post the 2011 perihelion passage and through the *Stardust-NExT* encounter on 14 February, 2011.

2.1. Correction for solar phase angle brightness effects

Li et al. (2007) have determined the disk integrated phase function of 9P to be $\beta = 0.046 \pm 0.007$ mag./deg for $4^\circ < \alpha < 117^\circ$. Earlier Belton et al. (2005a), using data obtained between 1997 and 2002, found evidence for an increase in β inside of 4° . They represented the phase law as a polynomial ($\Delta R(1,1,\alpha) = -0.0180955 - 0.250260\alpha + 0.0306201\alpha^2 - 0.021805\alpha^3 + 0.0000798\alpha^4 - 0.0000015\alpha^5$ mag.) good for $\alpha < 15^\circ$. In Fig. 2 the data and these two phase laws are compared, but, as can be seen, a simple linear regression, $R(1,1,\alpha) = 14.905 + 0.045\alpha$ mag, gives an excellent account of the current data for $1^\circ < \alpha < 14^\circ$. It is this latter relationship that we have used to correct the magnitude data to zero solar phase angle (Fig. 3).

In Figs. 3–5 we show $R(1,1,0)$ as a function of calendar year, time from perihelion passage, and heliocentric distance. In Fig. 3 we see how well the solar phase angle brightness effect has been removed. The scatter in magnitudes while the comet is near aphelion now primarily reflects the variation in brightness caused by the spin of 9P's irregularly shaped nucleus. In Fig. 4 we see how consistent the data are from one perihelion passage to the next. In Fig. 5 we see how the brightness of the coma is maintained at higher levels post-perihelion relative to its behavior pre-perihelion, an effect seen in other comet light curves and that prevented our use of early post-perihelion observations in the determination of the rotational state.

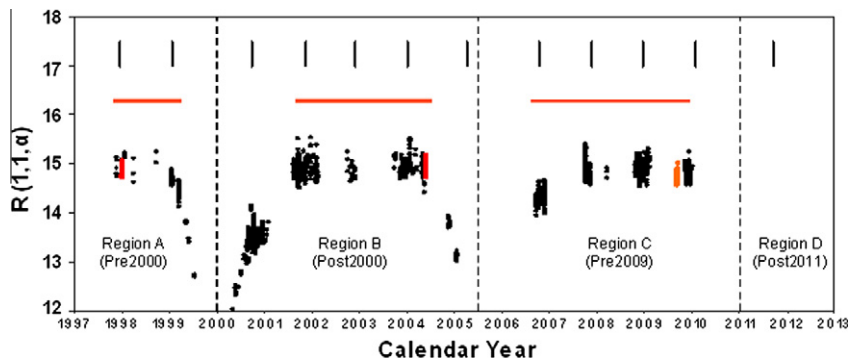


Fig. 3. $R(1,1,0)$ versus calendar year. The magnitude data have been corrected to zero phase angle using a linear phase law of 0.045α mag/deg. The flat trend around the time of each aphelion passage indicates that coma there is negligible and the scatter in that region is almost entirely due to the spin of the nucleus. The red circles denote HST data. The horizontal red bars shows the range of data in each region that was used in the rotational analysis.

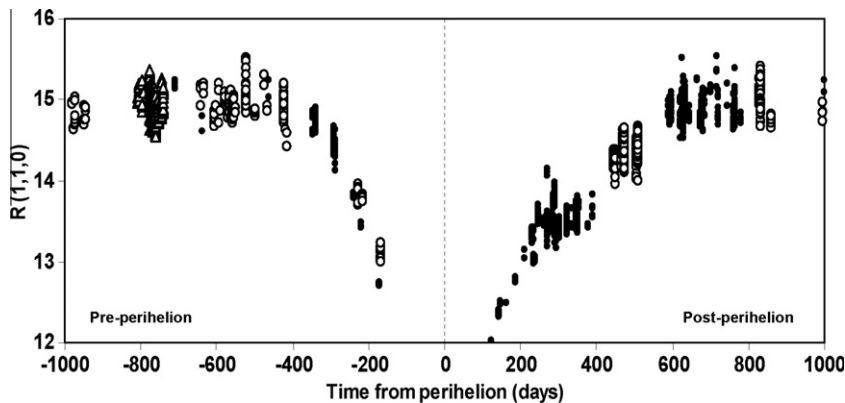


Fig. 4. $R(1,1,0)$ versus time from perihelion passage. The filled points are relative to the January 2, 2000, perihelion passage and the open circles are relative to the July 5, 2005, perihelion passage. The open triangles were taken in the fall of 2008 and refer to the 2011 perihelion. This figure shows the repeatability of the data from one perihelion to the next and also the asymmetry of the light curve about perihelion (see also Fig. 5).

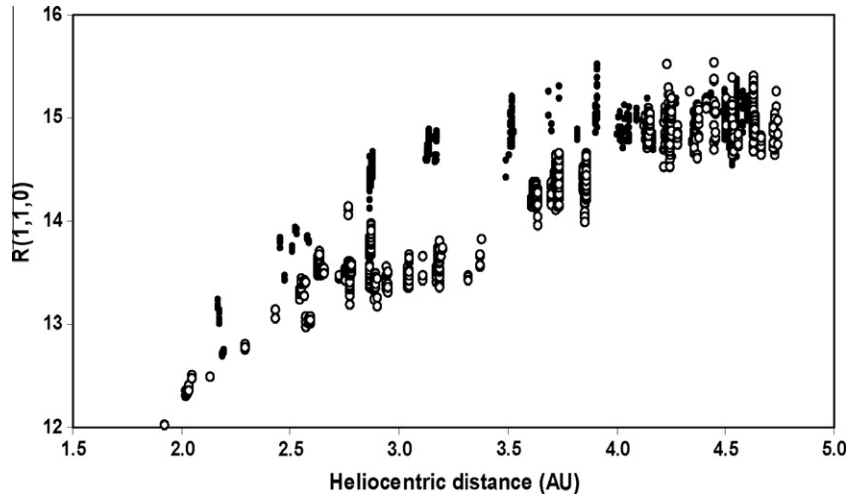


Fig. 5. $R(1,1,0)$ versus heliocentric distance. The brightness asymmetry about perihelion is clearly evident. The filled points are pre-perihelion, the open circles are post-perihelion. Notice that the mean trend becomes independent of heliocentric distance beyond 4 AU, indicating that light scattered from the nucleus dominates the signal.

2.2. Methods and preparation of the data for rotational analysis

Because of our intention to use the results of this study to adjust the arrival time of the *Stardust-NEXT* spacecraft at the comet (and so meet Level 1 requirements specified by NASA) it was decided to perform two independent analyses for the predicted rotational state of the comet. While the details of each of these are reserved to a later section, we now give an overview of these independent techniques as an introduction.

The first was done at the Jet Propulsion Laboratory in Pasadena and was based on a least-squares fit of model light curves to each region of $R(1,1,0)$. The model light curves were generated using a combination of the Thomas et al. (2007) shape model, a Hapke photometric function, SPICE orbital data (http://naif.jpl.nasa.gov/naif/data_comet.html), and an unexcited rotation model, i.e., the spin axis was assumed fixed in space and coincident with the principal axis of maximum moment of inertia. Hapke parameters for 9P have been determined by Li et al. (2007), however, in certain applications that utilized intensive computations, a Lommel–Seeliger (L–S) function was substituted. The L–S photometric function represents single (isotropic) scattering from a semi-infinite medium and comparisons with Hapke calculations demonstrated that it was an excellent proxy for 9P which has a low surface albedo.

The second investigation, which was done in parallel with that at JPL, was done at Belton Space Exploration Initiatives, LLC, in Tucson. This study applied standard astronomical period finding techniques to $R(1,1,0)$ after removing orbital synodic, solar phase angle timing (Harris et al., 1984), and light time effects. The data set was transformed to one that would have been acquired by an inertial observer fixed relative to the comet. This analysis avoided the use of the shape model and the choice of a surface photometric function. Under normal circumstances cometary light curve data rarely extend over an interval longer than two or three months near a single opposition and such observations can be phased to determine an adequate approximation to the rotational period without first accounting for orbital synodic effects or worrying about a change in the timing of light curve maxima due to changing illumination geometry (Fig. 6). In fact, these corrections would be hard to make without prior knowledge of some of the physical properties of the nucleus. In the present case, such prior knowledge is available, i.e., the rotational period, the polar axis, the shape, and photometric behavior of the nucleus are all approximately known (Belton et al., 2005a; Thomas et al., 2007; Li et al., 2007) and first order corrections can be made. Since the observations are, as shown in Fig. 7, spread over several oppositions that are widely separated around the orbit and involve a wide range

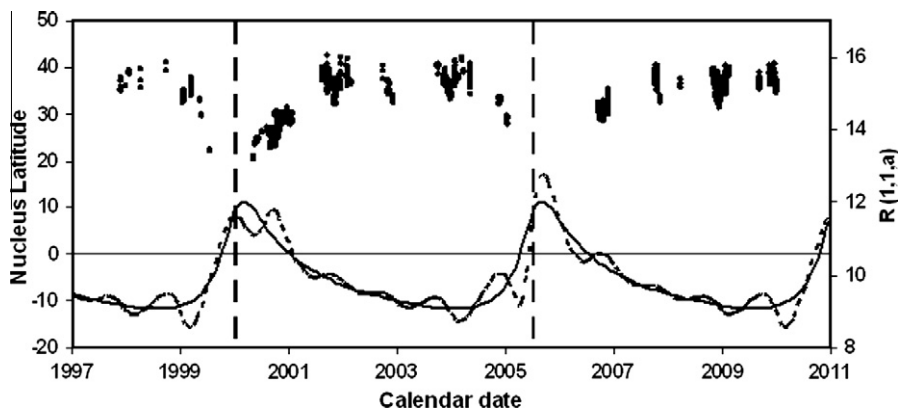


Fig. 6. Sub-solar (solid line) and sub-Earth (dashed line) latitudes (left ordinate) for 9P/Tempel 1 from 1997 to 2011. The data, $R(1,1,\alpha)$, are also shown (right ordinate). The sub-Earth latitude varies from -5° at the 2002 opposition to -14° at the 2004 opposition and this change of viewing geometry has an effect on the shape of the light curve. The increase in sub-Earth and Sun latitudes from negative to positive just prior to perihelion passage is important in the interpretation of H_2O productions rates (Schleicher, 2007) and consequently the torques on the nucleus (see Section 6).

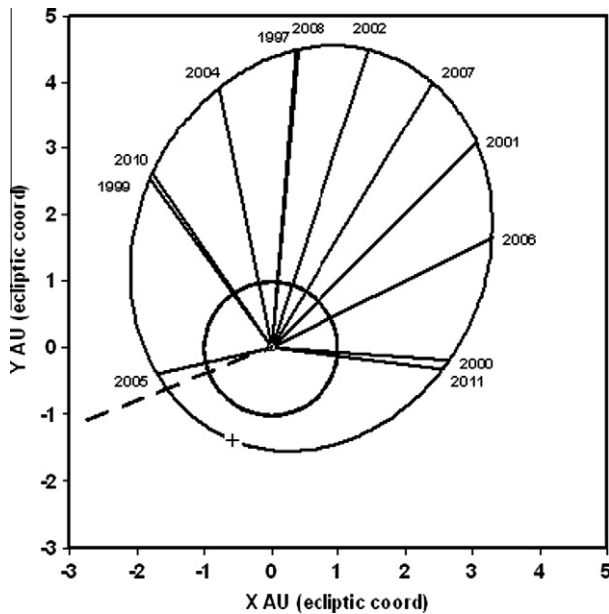


Fig. 7. The orbits of 9P/Tempel 1 and the Earth projected onto the ecliptic (since the comet's orbital inclination is low, its true orbit rises above the plane of the figure by, at most, 0.482 AU). Shown are the directions of the comet from the Sun at each opposition covered by the data. The wide spread of these directions shows why timing corrections must be made to the observations if the data from different oppositions are to be phased together and a sidereal rotation period determined. Also shown (dashed line) is the projection of the direction of the ascending node of the nucleus equatorial system ($\lambda_n=202.03$, $\beta_n=9.24$) that is used as a basic reference direction towards the nucleus when making corrections for synodic and illumination effects.

of solar phase angles, accounting for these effects is essential to obtaining well-defined light curves and in achieving the highest accuracy in the sidereal spin rate.

Both of these investigations were subjected to periodic and independent peer reviews during the analysis. The internal peer review team included A. Harris, T. Duxbury and D. Scheeres.

3. Deep Impact approach photometry

As noted in the introduction a number of estimates have been made of the rotational period of the nucleus based on the *Deep Impact* approach photometry. However, all of these were based on an early form of the photometry that was subsequently found to have short-comings that may have affected the results in the earliest parts of the approach sequence. These problems, which could possibly affect the accuracy of the estimated period, include estimation of the bias correction to the nearest DN (data number, a linear measure of the brightness), ignoring faint horizontal striping in the images, and ignoring small corrections to the photometry that are required when the comet happened to be placed on the two rows in the image surrounding the horizontal boundary between the upper and lower halves of the detector. These corrections have now been made (see Appendix A for a more complete discussion) and a new, improved, version of the approach photometry made available for analysis. It consists of 595 points of “science” data covering 63.1 dy on approach and 2419 points of “navigation” data covering an interval of 49.8 dy. The last datum in these sets was taken at 0.25 dy before impact. All data considered here (2888 Science and Navigation observations taken from 50 to 0.25 dy before impact) were taken with the Medium Resolution Instrument (MRI) through one or the other of two CLEAR, effectively identical, filters with a central wavelength at 650 nm (Hampton et al., 2005). The photometry, which refers to circular

apertures 5, 7, 9, 15, 20, 25, and 30 pixels in diameter centered on the comet, can be found on the PDS Small bodies Node <http://pdssbn.astro.umd.edu> in the *Deep Impact* archives.

We assume that the light of the nucleus, which was centered in the circular aperture, was completely contained within it. At 0.25 dy before impact (the last datum) the mean diameter of the nucleus subtends 1.8 pixels; i.e., the nucleus is always within our smallest aperture of 5 pixels. The DN at each time, t , consists of two parts: that contributed by the nucleus and that by the inner coma. We express the signal as:

$$DN(t) = AC_n f_n(\alpha) F_n(t) r^{-2} \Delta^{-2} + F_c(t, r, \Delta, \alpha) \quad (1)$$

where A is a constant calibration factor, C_n is the mean brightness of the nucleus, and f_n is the solar phase function (as determined in Section 2). $F_n(t)$ is the variation of the brightness of the nucleus as it rotates, and r and Δ are the distances from the Sun and the spacecraft in AU. F_c is the coma contribution to the signal and has a complex dependence on the parameters shown. With the exception of A , F_c and F_n all of the other quantities are specified. Our objective is to determine the product $A \cdot F_n$ and analyze its time dependency for the rotational period. To do this we must first separate $A \cdot F_n$ from F_c , which we assume to make a negligible *rotational* contribution to the signal. Unfortunately, this latter assumption cannot be precisely true since the origin of coma material is tied to the surface of the nucleus and will initially share its motion. As the coma material flows out from the nucleus conservation of angular momentum will reduce its angular motion and periodicities may be introduced that are systematically different from that of the nucleus.

We have investigated the possible effect of this phenomenon by searching for coma variability in the difference signal between the 7 and 5 pixel apertures. This signal should arise entirely from the coma. For times close to impact, when the very inner coma is being sampled, we have detected variability at the nucleus period but with an amplitude that is ~ 0.1 that of the variability of the nucleus itself. At 10 dy before impact, when a more distant and broader region of the coma is being sampled, coma variability is undetectable presumably being overwhelmed by noise. At 0.25 dy before impact, the coma signal in the 5 pixel aperture is only ~ 0.04 that of the nucleus (Fig. 8), and so the amplitude of the coma's observed variability contributes a negligible ~ 0.004 fraction of the total observed amplitude. At earlier times, well before impact and when the coma is the dominant component of the signal, the 5 pixel aperture integrates over a wide region of the coma presumably washing out any rotational variability from that source. In Fig. 8 we show the approximate contribution of the nucleus to the total signal in the 5 pixel diameter aperture. This first order separation of the nucleus from the coma was done by assuming that there is a linear relationship between the coma signal and aperture diameter (D) in apertures 5 through 30. The signal extrapolated to $D=0$ is a first order estimate of the contribution of the nucleus. This simple coma model is based on a symmetric constant velocity outflow in the

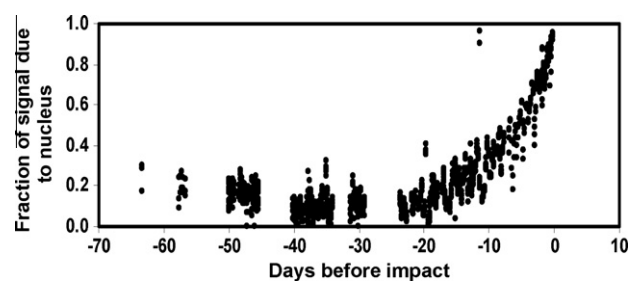


Fig. 8. Fraction of signal due to the nucleus in each data point of the *Deep Impact* approach photometry. Evidently coma dominates the photometric signal for most of the data until about 4 days before impact (see text for a detailed explanation).

coma and a point nucleus and predicts the roughly linear dependence of the signal with aperture size that is seen in the data. The coma is seen to dominate until about 4 days before encounter, and considerable care was taken to remove it before the rotational analysis.

The data consist of two groups: “Science” data and “Navigation” data whose time coverage, sampling, and mode of acquisition were quite distinct. While they are taken with the same instrument and filters they were taken in different camera modes as described in Appendix A. Nevertheless, the two types of data were found to be photometrically consistent and we use them together as a “joint” data set. To illustrate the separation of coma from $A \cdot F_n$ and the “cleaned-up” data, we plot in Fig. 9 the normalized brightness, $r^2 \Delta^2 \text{DN} / C_n f(\alpha)$, versus time from impact of the signal in the 5 pixel aperture photometry. C_n is taken as 100 units and r , Δ , and α were obtained from the JPL Horizons system where the *Deep Impact* spacecraft is identified as “@ - 140”. The coma and mean nucleus brightness is represented as a 4th-order polynomial in each of the two cleaned-up data sets and then subtracted leaving the time variable component of the nucleus, $A \cdot F_n$. In principle the mean level of this component should be constant and zero and this can be seen to be approximately the case in Fig. 9. The two data sets are then combined to form the joint version of $A \cdot F_n$ shown in the lower panel of the figure.

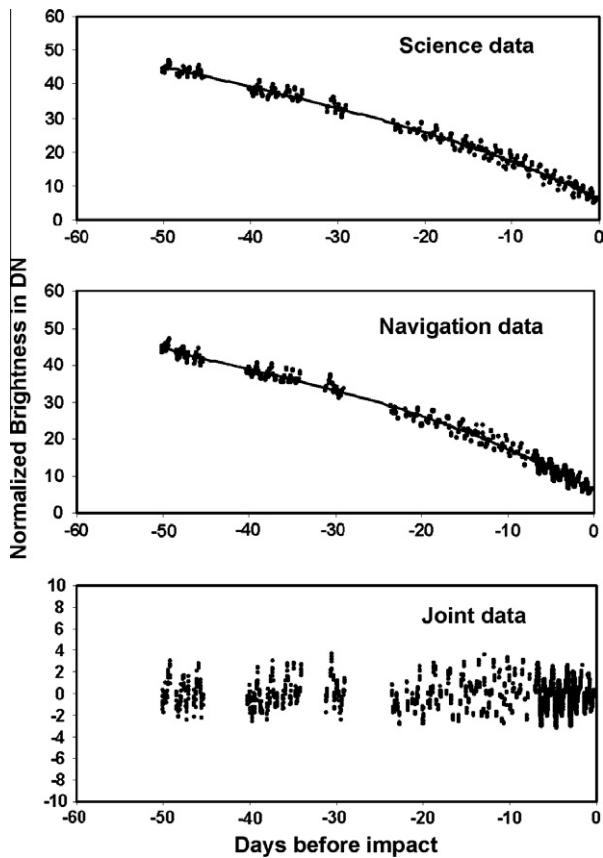


Fig. 9. *Deep Impact* approach photometry. The top two panels show a normalized version of the science and navigation data separately after the clean-up process that removed variability due to mini-outbursts (Farnham et al., 2007; Belton et al., 2008). The data, in ‘data numbers’ (DN), are normalized by the factor $r^2 \Delta^2 / C_n f(\alpha)$ as described in the text. Also shown are 4th-order, least-square fit, polynomials fitted to the data. These represent the general run of the sum of the underlying coma signal and the mean nucleus signal. In the lower panel is the difference between the data and the polynomials, which is taken to represent the rotational variability of the nucleus.

4. Rotational equations of motion and assumptions

The action of forces generated by the momentum of gas leaving the surface of an active comet nucleus can at any instant of time be decomposed into two parts: those which act at the center of mass of the body, \mathbf{F} , and those which apply torques, \mathbf{T} . Both forces are functions of time, t , and vary rapidly on a rotational time scale but are thought to vary relatively smoothly on an orbital time scale.

Occasionally major cometary events such as a splitting, or a major outburst, or the appearance or disappearance of a major active region, or a close encounter with a major solar system body may occur that lead to unpredictable changes in these forces. Such effects are not considered here since no such major events were observed for this comet for the time covered by the observation used in this paper and we assume that the rate of change of the average of $\mathbf{T}(t)$ over a rotational cycle, $d \langle \mathbf{T}(t) \rangle / dt$, changes smoothly over orbital timescales. It is not necessary that such orbital changes are the same from one orbit to another and we shall, in fact, find that they are not.

We assume that the nucleus rotates as a rigid body and the vector equation for the angular motion of such a body in a fixed frame, e.g., Rutherford (1951), is:

$$d\mathbf{h}/dt = \mathbf{T}_{\text{tidal}}(t) + \mathbf{T}(t) \quad (2)$$

where \mathbf{h} is the angular momentum of the body and $\mathbf{T}_{\text{tidal}}$ are torques that come into play during near encounters with planets or the Sun. In the present application we shall assume that $\mathbf{T}_{\text{tidal}} \equiv 0$. The net torque due to mass loss is therefore defined as:

$$\mathbf{T} = \int (\boldsymbol{\rho} \times q\mathbf{V}) dS \quad (3)$$

where $\boldsymbol{\rho}$ is the position vector of an elemental area dS with respect to the center of mass of the nucleus. Here \times is a vector product. $\mathbf{V}(t)$ is the velocity of the outflow and $q(t)$ is the net rate of mass loss across dS . The integration is over the entire surface and, although not specifically indicated in the notation, averaged over a rotational cycle. With $\boldsymbol{\omega}$ as the angular velocity of the nucleus relative to fixed axes that momentarily coincide with the principle axes of inertia of the nucleus, Eq. (2) yields Euler’s equations of angular motion:

$$\begin{aligned} A^* d\omega_x/dt + (C^* - B^*)\omega_y\omega_z &= [\int \boldsymbol{\rho} \times q\mathbf{V} dS]_x \\ B^* d\omega_y/dt + (A^* - C^*)\omega_z\omega_x &= [\int (\boldsymbol{\rho} \times q\mathbf{V}) dS]_y \\ C^* d\omega_z/dt + (B^* - A^*)\omega_x\omega_y &= [\int (\boldsymbol{\rho} \times q\mathbf{V}) dS]_z \end{aligned} \quad (4)$$

where A^* , B^* , and C^* are the principal moments of inertia.

The assumption that a cometary nucleus rotates as a rigid body deserves some comment in light of the low cohesive strength found for cometary material in D/Shoemaker–Levy 9 (Asphaug and Benz, 1996) and 9P (Richardson et al., 2007) and the proposition of Belton and Melosh (2009) that fluidized transport of substantial amounts of material may take place episodically in the interior ultimately leading to outbursts and surface flows. To justify our assumption it is sufficient to show that rotation is a minor source of stress and that the loss of material in a repetitive outburst has a minor effect on the moment of inertia. Near the ends of the long axis of 9P the gravity is $\sim 0.027 \times \text{cm/s}^2$, and the centripetal acceleration is $\sim -0.001 \times \text{cm/s}^2$ thus the rotational contribution is minor. We estimate the moment of inertia of the nucleus to lie between 0.8 and $4.6 \times 10^{19} \text{ kg m}^2$ assuming a homogeneous mass distribution in the interior, a spherical approximation to the shape, and using the mass range determined by Richardson et al. (2007). A typical repetitive outburst releases about 10^6 kg of material at the surface whose maximum contribution to the moment of inertia for a 3 km radius body is $\sim 10^{13} \text{ kg m}^2$. Since this contribution is many orders of magnitude less than the moment of inertia,

the loss of material in a repetitive outburst, or similar events, will not have a noticeable effect on the rotational dynamics of the nucleus.

These equations provide a firm basis for detailed *ab initio* simulations of the evolution of the spin of the nucleus, if the inertias and mass loss are fully understood e.g., Samarasinha and Belton (1995) or Gutiérrez and Davidsson (2007). The study of non-gravitational effects on 9P's orbit suggest that the direction of the spin axis is stable or, at most, slowly changing (Yeomans et al., 2004b). In addition, the close similarity of the pole direction (RA, Dec = 294°, +73°; J2000) found by Thomas et al. (2007) from *Deep Impact* images of the resolved nucleus with the pole direction (RA, Dec = 293°, +73°) derived from the time dependence of coma features by Vincent et al. (2010) suggests that the direction of the polar axis is well determined. In addition the constant pole direction (RA, Dec = 46°, +73° revised to 317°, +81° in 2006) derived from light curves obtained over several years prior to the *Deep Impact* encounter (Belton et al., 2005a) support the idea that any precessional drift in the pole direction is slow, i.e., not exceeding a few degrees on the sky per perihelion passage. Moreover, with the assumption of a homogeneous mass distribution in the nucleus, observations of the shape of the nucleus allow us to estimate the direction of the principal axis of maximum moment of inertia, which, within the errors of estimation, is found to be parallel and coincident with the estimated spin axis (Thomas et al., 2007). All of these observations support the idea that the spin of the comet is close to its fully relaxed state. Additional support comes from an analysis of periodicities in the *Deep Impact* light curve, which is found to yield only harmonics of a single period. While this does not ensure that the nucleus is in a fully relaxed state it is, nevertheless, a necessary condition. We conclude that the nucleus is apparently close to the state of simple rotation around its principal axis of maximum moment of inertia, which we take as C^* . In this case the z-axis is coincident with the spin axis and we assume that $\omega_x = \omega_y = d\omega_x/dt = d\omega_y/dt = 0$. This assumption implies that, for over the period of the observations being considered, the direction of the rotation axis is considered fixed. We will revisit and provide a check on this assumption in Section 6.

After dropping the z subscript, Eq. (4) reduce to:

$$d\omega(t)/dt = T(t) \quad (5)$$

where

$$T(t) = \left[\int (\boldsymbol{\rho} \times q\mathbf{V}) dS \right]_z / C^*$$

averaged over a rotational cycle.

We define the *rotational phase*, $W(t)$, of the nucleus at time, t , as the angular distance of the prime meridian, as defined by Thomas et al. (2007), to the meridian that contains the direction of the ascending node (RA, Dec = 23.80°, 0.0°; J2000) as seen from the nucleus, i.e.,

$$dW(t)/dt = \omega(t) \quad (6)$$

The ascending node is at the intersection of the nucleus equator and the celestial equator. Also, for reference, the obliquity of the spin axis, i.e., its angle with the orbital plane, is 11.9°. Integrating from t_0 to t , we get

$$W(t) = W_0 + \int_{t_0,t} \omega(t) dt. \quad (7)$$

Since the sense of spin of 9P is observed to be *direct* (Thomas et al., 2007), $W(t)$ is the West longitude of the reference direction at time t . At the time of impact in the *Deep Impact* Mission (JD 2453555.73928) Thomas et al. (2007) found that

$$W(t) = 252.63^\circ + 212.064(t - t_0) \quad (8)$$

where the standard epoch is $t_0 = \text{JD } 2451545.0$ and the assumed spin rate ($212.064^\circ/\text{dy}$) was constant between the standard epoch and the time of impact.

In the analysis that follows we make two further assumptions. First, we assume that for an extended period around aphelion (within Regions A–D) $d\omega/dt = 0$, i.e., torques during that period are negligible. Secondly, we assume that the light curve of the nucleus, in the same extended period around aphelion, can be predicted from Thomas et al.'s (2007) shape model. Referring to Eq. (7) and Fig. 3, the first of these assumptions implies that the following relationships exist:

$$W_j(t) = W_{0j} + S_j * (t - t_0), \quad j = \text{Regions A–D} \quad (9)$$

and the rotational analysis in the next section is designed to discover W_{0j} and S_j for each of the regions.

The second of the above assumptions is more problematical because the three-dimensional shape of 9P's nucleus is poorly defined over large areas. This deficiency is a direct result of the linear *Deep Impact* flyby geometry and the slow rotation of 9P. Tests of model predictions with *Deep Impact* approach photometry show that with either a Lommel–Seeliger or Hapke scattering function the Thomas et al. (2007) shape model can give a good match to the observations. However, while the shape model gives good results for the light curve at most rotational phases, we find that there is a restricted range of rotational phase (see Section 5) where the data and models are discordant.

The validity of both of the above assumptions depends on the premise that there is an extended interval near aphelion when the effect of coma on the light curve and the dynamics of the nucleus is negligible. To assess the influence of the coma we first remove the mean brightness of the nucleus from the data shown in Fig. 3. The mean absolute R magnitude of the nucleus at zero solar phase angle is taken as 14.905 (see Section 2 for the origin of this value) and magnitudes are converted to relative brightness units with the mean brightness of the nucleus set at 100 units. In Fig. 10 the pre- and post-2005 perihelion coma brightness is compared to the mean brightness of the nucleus (shown as a dashed horizontal line). Pre-perihelion the signal is essentially coma free at distances beyond 3.2 AU where the RMS variability of ± 15 units is mainly due to rotation. The error of an observation is typically ± 3.5 units. In the post-perihelion period only the data beyond 4.1 AU can be considered free of coma. The RMS spread at these distances is again ± 15 units. The post-perihelion data between 3.6 and 3.9 AU are from the 2006 opposition and are $\sim 42\%$ due to coma. However, the RMS variation of ± 17 units is roughly similar to the mean level found beyond 4.1 AU suggesting that the variability in 2006 remains dominated by rotation. A substantial observational effort was made during the September 2000 opposition to obtain rotational information when the comet was near 3 AU post-perihelion. However, at that time the coma level was 2.7 times that of the nucleus and the RMS spread had increased to ± 55 units. Since the signature of nucleus rotation is expected to be at the ± 15 unit level, it is clearly overwhelmed by variability in the coma. We have therefore omitted this part of the data from the rotational analysis.

5. Rotational analysis

We determine the values of W_{0j} and S_j (Eq. (9)) for each Region j using the two methods described earlier. They share identical data sets, and the combined ground-based and *HST* data for each region are shown in Fig. 11. The *Deep Impact* data are already displayed in the bottom panel of Fig. 9. Descriptive information on the data is collected in Table 1.

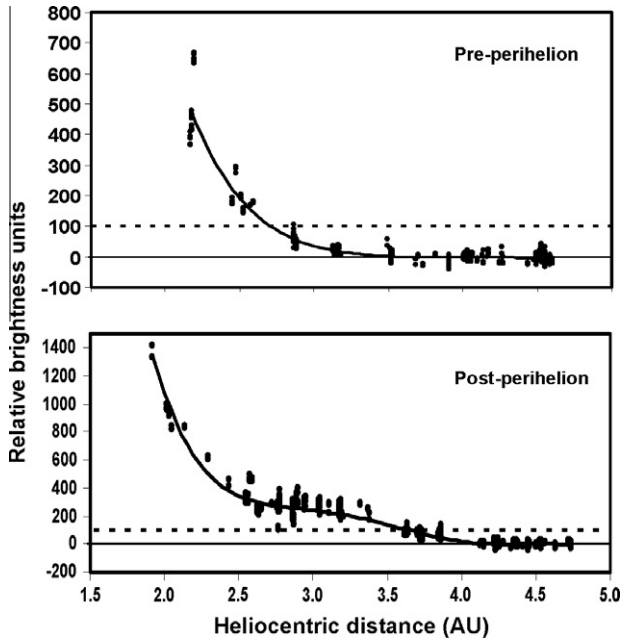


Fig. 10. Plots of pre- and post-2005 perihelion brightness as seen from the Earth in relative brightness units (mean nucleus brightness = 100 units) after the mean brightness of the nucleus has been removed. The dashed horizontal lines show the mean brightness of the nucleus for comparison purposes. These plots make it easy to evaluate the relative contributions of the coma and nucleus to the total brightness and determine the heliocentric distances between which the production of a coma is insignificant, i.e., from 4.1 AU post-perihelion to 3.2 AU pre-perihelion. The curves are polynomials, which, as can be seen, only approximately represent the run of the coma levels. They are not used in the analysis and are shown only to indicate the general trend of coma brightness.

5.1. The JPL method

This method is simply a classical least-squares fit (technically a square-root information filter) of a rotation model to the measured photometry. For the more typical case of unaccelerated rotation, which is presumed between active periods, the model parameters are the rotation phase $W_{0j} = W_j(t_0)$ and rate $S_j = S_j(t_0)$ at some epoch t_0 . In this way the spin phase and rate were obtained from a simultaneous fit to the photometry, in contrast to the power spectrum analysis used in the Tucson method described below.

The least-squares approach attempts to minimize the sum of squares of the photometric residuals, which are the differences between the observed and computed (O–C) magnitudes of the cometary nucleus at each measurement time. The observed photometry is reduced to R(1,1,0) values, while the computed magnitudes are obtained from special-purpose synthetic light curve generation tools that compute the brightness from the shape model (“runlcrv.cgi” and “runlcrv_hapke.cgi” provided by B. Carcich) that can be queried online.

The synthetic light curve tool takes as input the rotation history of the comet based on the assumed values of W_{0j} and S_j and returns

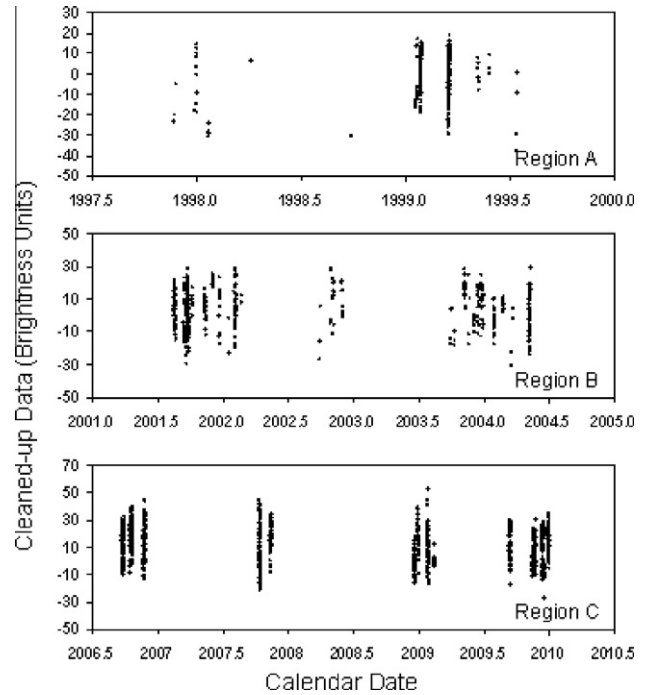


Fig. 11. Brightness data for 9P/Tempel 1 used in the rotational analysis. The data are shown after the clean-up process (see text) and displayed as a function of observing time. The three observing regions defined in Fig. 1 are shown separately. The mean brightness of the nucleus (100 units) has been removed.

the received flux at a list of requested observation times for a specified observing location. The position of the observer can be selected as the geocenter, *Deep Impact* spacecraft, *Stardust-NExT* spacecraft, *Spitzer Space Telescope* or *Hubble Space Telescope*. These tools use Lommel–Seeliger and Hapke scattering laws and the Thomas et al. (2007) shape model. They use a plate model (Miller, 1995–Private communication) for the comet shape to capture the illumination effects for the particular positions of the observer and the Sun at the emit time, and the light time delay is fully incorporated in order to accurately represent the measured flux at the observation time, i.e., receive time. We used a plate model having vertices on $\sim 6^\circ$ centers, which we found to be a suitable compromise between performance and fidelity. Fluxes were converted to generic magnitudes and the optimal offset to R-band was also estimated. Some individual batches of photometry also required the estimation of an independent, *ad hoc* magnitude offset, typically due to coma contamination issues.

The least squares fitting process converged well when near a local minimum, but nonlinearities often led to large corrections when the initial guess was far from the minimum. Thus special care was needed in slowly building up to a global fit to larger data sets, e.g., an entire quiescent period. A typical fitting approach was to estimate the spin state with a short (few to several days) but relatively dense data set, where the light curve variation was clearly

Table 1
The data used in the rotational analysis.

Region	Number of observations	Time span (days)	Standard deviation ^a	Heliocentric ^b range (AU)	Dates
A	307	600	±11	4.5–2.2	11/23/97–7/15/99
B	541	1000	±12	4.1–3.5	8/16/01–5/11/04
DI	2888	50	±23	1.6–1.5	5/15/05–7/3/05
C	1074	1194	±13	3.6–3.3	9/24/06–12/30/09

^a In brightness units; the mean nucleus brightness = 100 units. The large standard deviation in the *Deep Impact* data is due to noise from the coma that was present in the signal.

^b For Regions A–C the heliocentric range passes through aphelion at 4.74 AU.

visible. The epoch t_0 would be situated within this data set (Fig. 12). Adding more and more data to slowly extend the fit span occasionally yielded good results, but in many cases the measurement gaps were too large to prevent ambiguities in the number of intervening rotations. An alternate method was to fix the rotation phase obtained from the short, dense data set and then scan a wide range of rotation rates to see which ones fit the larger data set the best. This approach yielded something akin to the periodograms used in the Tucson approach, but which had a somewhat different origin and interpretation (Fig. 13). With this approach we could generally identify a single or perhaps a few candidate frequencies that could be considered more carefully.

Overall, fits were generally acceptable, but as can be seen from Fig. 17, the model light curve did have a significant departure from

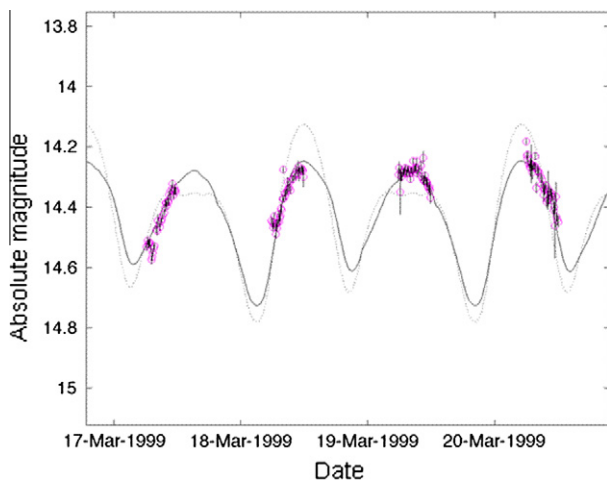


Fig. 12. An example of the fit of data in the JPL analysis over a limited interval around an assumed t_0 (in this case Region A) to the predicted model light curve (black line). Abscissa is in magnitudes with arbitrary origin.

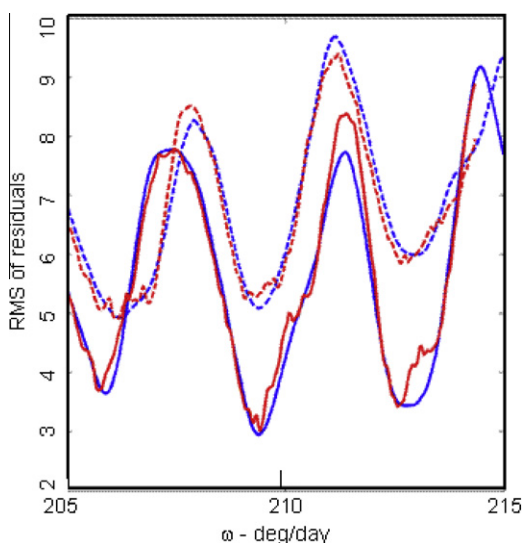


Fig. 13. An example of an alternate method to determine the spin rate used in the JPL analysis where the RMS of residuals are minimized by estimating only the rotation phase over a range of fixed spin rates (ω). Dashed and solid curves distinguish the 180° ambiguity in rotation phase, with the solid curves indicating the preferred orientation. Blue curves are for fits to a short, dense data set (March 1999 only) while the red curves are for fits to the entire Region A data set (1997–1999).

the measured light curve. This discrepancy was associated with illumination of regions where the shape model is not well constrained by the *Deep Impact* approach photometry. However, the fitting process need only fit the gross features of the light curve and so mismodeling of the light curve was not a serious obstacle to estimating the rotation state, aside from the 180° phase ambiguity discussed in Section 5.2.

5.2. Ground-based photometry

This large data set, described more exhaustively by Meech et al. (2011, in press), formed the foundation for all of the quiescent fits in Regions A–C. Most of the photometry obtained while the comet was highly active was not usable for rotation estimation, but many good batches even with substantial coma contamination were found to be helpful. For the JPL method, isolated individual observations contributed little to rotation knowledge, but the numerous batches (e.g., Fig. 12) showing clear light curve variation and slope from night to night proved to be vital.

5.3. Deep impact photometry

The densest set of photometry available for this study was that derived from the approach photometry from the *Deep Impact* mission. This data set followed the model light curve with excellent coverage over seven weeks (Fig. 14) and, moreover, it was obtained while the comet was active and the spin state was presumably accelerating. With this in mind, we extended our rotation model to estimate the angular acceleration of the comet during the *Deep Impact* approach and found that the comet was indeed spinning up during this time. The acceleration model applied a torque proportional to the sublimation rate of water, as given by the $g(r)$ function commonly used to model non-gravitational accelerations on comets (Marsden et al., 1973). This approach allows the acceleration to build slowly, reaching a peak at perihelion and then fading back to effectively zero around 2.5 AU post-perihelion. As we explain below, the comet acceleration profile was rather more complex, but we were still able to use this simpler model to estimate the acceleration on the relatively short interval of the *Deep Impact* approach. Specifically, we find that the best-fitting acceleration according to this model is $dS/dt = A * g(r)$, where $A = 0.0789 \pm 0.0031^\circ/\text{dy}^2$. Thus formal uncertainty is only about 4%, and so the estimated acceleration is non-zero with very strong statistical significance. This model indicates an acceleration starting at $0.024^\circ/\text{dy}^2$ at the beginning of the *Deep Impact* data set and reaching $0.028^\circ/\text{dy}^2$ by the end of the data set about a day before perihelion. This model was eventually superseded by the acceleration profiles described in Section 6.

5.4. Hubble Space Telescope and Spitzer photometry

Photometric observations of Tempel 1 taken by the *Hubble Space Telescope* were obtained in 1997 (Lamy et al., 2001, 2007) and 2009 (Meech et al., 2011, in press) Each of these data sets proved crucial in establishing the spin state in Regions A–C because of the dense coverage and high SNR that unambiguously showed the light curve morphology. *Spitzer* flux measurements (Lisse et al., 2005) were converted to magnitudes and compared with predictions for visible magnitudes. While we chose not to actually fit these data due to uncertainties about the relative shape and phasing of light curve extrema, we found that the placement of observed *Spitzer* extrema did agree well with those predicted for visible extrema. The agreement in phase between the *Spitzer* thermal IR light curve and the visible light curve also support the basic assumption made in this paper that the visible light curve is controlled primarily by the shape of the nucleus.

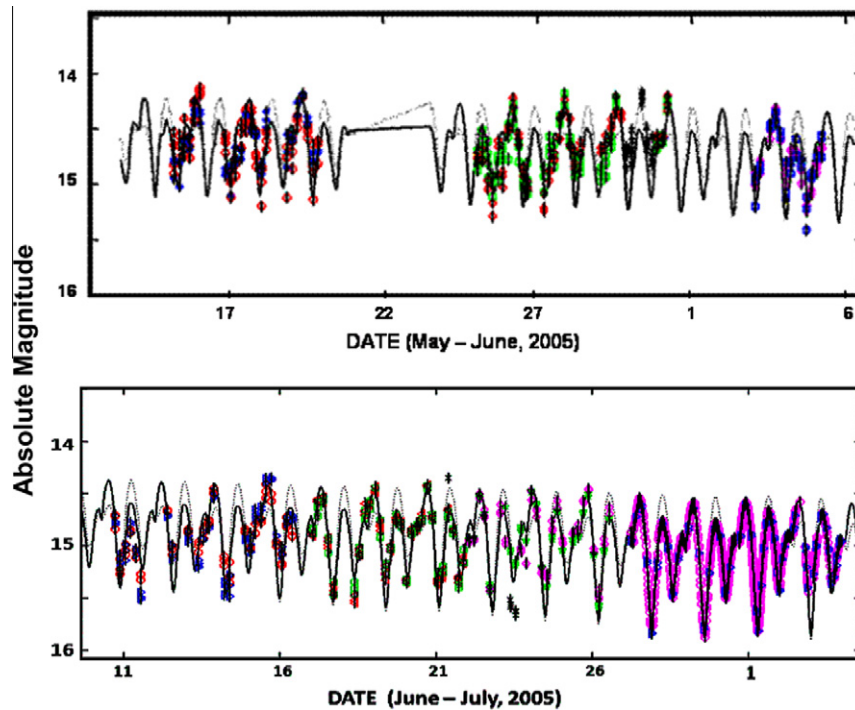


Fig. 14. Model light curve fits to the Deep Impact approach photometry in the JPL analysis. The dark black line is for the Hapke phase function. The colors of the data points represent the different data batches used in estimating the magnitude offset for that time period.

5.5. The Tucson method

The sidereal spin rates, S_j , are determined separately from the rotational phases, W_{0j} . They are determined without reference to model lightcurves and, to remove drift in the rotational phase of the observed light curve due to changes in the solar phase angle (Surdej and Surdej, 1978; Harris et al., 1984) and orbital motion, the observing times are adjusted to create a data set for each region as it would have been observed by a fictitious observer viewing the comet from the direction of the ascending node of the comet at zero solar phase angle. After correcting for light time, this approach ensures that periodicities in the modified light curve reflect the sidereal spin of the nucleus. Because of changing sub-solar and sub-observer latitudes at the elongated nucleus (Fig. 6), the shape of the observed light curve will not be consistent in amplitude, but, because of the low obliquity of the comet (11.9°), this effect is expected to be small. We do expect, however, that these changes will introduce some amplitude dispersion in the rotationally phased light curves.

Once the S_j are determined, the rotational phase in each region is then estimated by comparing model light curve predictions, based on the Thomas shape model and a Hapke phase function, to high S/N *Hubble Space Telescope* data. In the case of Region A, where the Lamy et al. (2001) *HST* data do not cover a full rotation period, ground-based data are also used in the determination of rotational phase.

5.6. Removal of synodic, solar phase angle, and light time effects

The observing time for a particular observation is first adjusted to zero solar phase angle using a variation of the Phase Angle Bisector (PAB) method of Harris et al. (1984). These authors note that as the solar phase angle increases from zero the rotational phase of the light curve drifts in the same direction but at approximately half the rate. Since the timescale for change in the solar phase angle, α , is much greater than the rotational period, the rotational

phase $W_j(\alpha)$ of the observed light curve at solar phase angle α will be shifted by $\Delta W_j(\alpha) = \beta(\alpha/2)$ from its value at zero phase where β is the longitude interval between the meridian that passes through the sub-solar point and the meridian that includes the PAB. $\Delta W(\alpha)$ corresponds to a timing correction of $\Delta t(\alpha) \approx P\Delta W(\alpha)/360$ where P is the estimated rotation period. Using the same logic the timing correction for the orbital position of the comet at time, t , is $\Delta t(\gamma) \approx P\Delta W_s(\gamma)/360$ where γ is the longitude interval between the meridian that contains the sub-solar point and the meridian that contains the ascending node. The total correction to the observing time is therefore $\Delta t = \Delta t(\alpha) + \Delta t(\gamma) + \Delta t(d)$ where $\Delta t(d)$ is the light time correction for an observer at a distance d from the nucleus. Δt varies considerably throughout the various observation sets and falls in the range of $0.81 > \Delta t > 0.20$ dy.

5.7. Preparation of the data for high precision frequency analysis

The data are first linearly detrended (this is a small correction as can be seen from Fig. 11) and a preliminary value of S_j is determined with the ANOVA (ANalysis Of Variations; Schwarzenberg-Czerny, 1996) period-finding algorithm in the commercially available *Peranso* software package (this is available at www.CBABELgium.com). We experimented with the thirteen period finding routines, which include all of the major astronomical period-finding algorithms, in the *Peranso* package plus the Window-CLEAN algorithm developed in our own group (Belton and Gandhi, 1988) on various subsets of the data and found that the ANOVA algorithm gave the clearest and most consistent results. Other often-used methods, such as FALC (Harris et al., 1989) and PDM (Stellingwerf, 1978), gave effectively identical results.

We have used the uncertainty estimates as calculated in the *Peranso* package. The method used is that described by Schwarzenberg-Czerny (1991) in which the uncertainty in the period is taken as the width of the associated peak at the mean noise level down from the peak.

Once the preliminary period estimates have been calculated they are used to rotationally phase the data so that they can be examined to estimate bias corrections for particular observing runs and remove obviously discordant outliers. In this way the data sets can be “cleaned-up.” This process, removes small systematic errors that may arise in cases of unresolved activity.

The cleaned-up data are then analyzed with the ANOVA algorithm a second time to obtain the final estimates of periodicities and uncertainties. This process yields our ‘best’ estimate of the period and its uncertainty in each observational region. While this two step process is not one that we would recommend for finding periodicities *ab initio* in an arbitrary data set, we have confidence in using it here because of the special knowledge produced by the *Deep Impact* encounter photometry, i.e., we know the approximate spin period and have a fair idea of the shape of the light curve, knowledge that we use to discriminate against spurious period estimates. ANOVA periodograms and cleaned-up rotationally phased light curves for the Regions A–C and the DI data are shown in Figs. 15 and 16 respectively.

5.8. Determination of rotational phases

To determine the rotational phase, W_{0j} , of the data in each observation region we have relied primarily on *HST* data, which, in Regions B and C, provide consistent and well-sampled coverage over a complete rotational cycle. The phase is tied into the Thomas et al. (2007) nucleus coordinate system by fitting the observed light curve to a model light curve computed from the Thomas et al. shape model using the online tool noted earlier. The final fits to the data are shown in Fig. 17. The accuracy of fit is estimated at $\pm 2^\circ$ in rotational phase by visual inspection. A detailed examination of Fig. 17 shows that there is a distinct possibility of a 180° ambiguity in rotational phase. We have used both numerical cross-correlation and visual inspection to decide the appropriate alignment of the model to the data. However, the results of both methods are, in our opinion, marginal. While both of these techniques support the choice of alignment that we advocate in this paper the possibility of a $\sim 180^\circ$ error in rotational phase must be entertained.

The fits in Fig. 17 show that the model fit is deficient in the range of rotational phase associated with the primary minimum of the observed light curve and that there is a possible ambiguity of 180° in rotational phase. The final estimates for S_j and W_{0j} are collected in Table 2 and the evolution of S_j with time is shown in Fig. 18.

5.9. Direct determination of the acceleration of the spin rate

Because the comet was active during the collection of the *Deep Impact* data we recognized that it could contain direct information on the acceleration of 9P/Tempel 1’s spin. We therefore applied the dynamical period estimation methods of Drahus and Waniak (2006), which simultaneously yield both a spin rate and its acceleration (assumed linear in this case) at the mid-time of the observations (Appendix B contains a detailed description of its application to the *Deep Impact* data). This estimate yielded a period of 1.69961 ± 0.00023 dy (40.791 h; $211.814 \pm 0.029^\circ/\text{dy}$) applicable at JD 2453530.60510 and a rate of change in the spin rate of $+0.020 \pm 0.003^\circ/\text{dy}/\text{dy}$. As can be seen in Fig. 18 this value is consistent with the period change through perihelion that we have found in the Earth-based data if the timescale over which the torque acts is ~ 63 days.

The JPL and Tucson approaches described here are substantially independent, and indeed complementary. Through the use of the light curve generation tool, the viewing geometry, phase angle correction and light time delay are automatically incorporated into

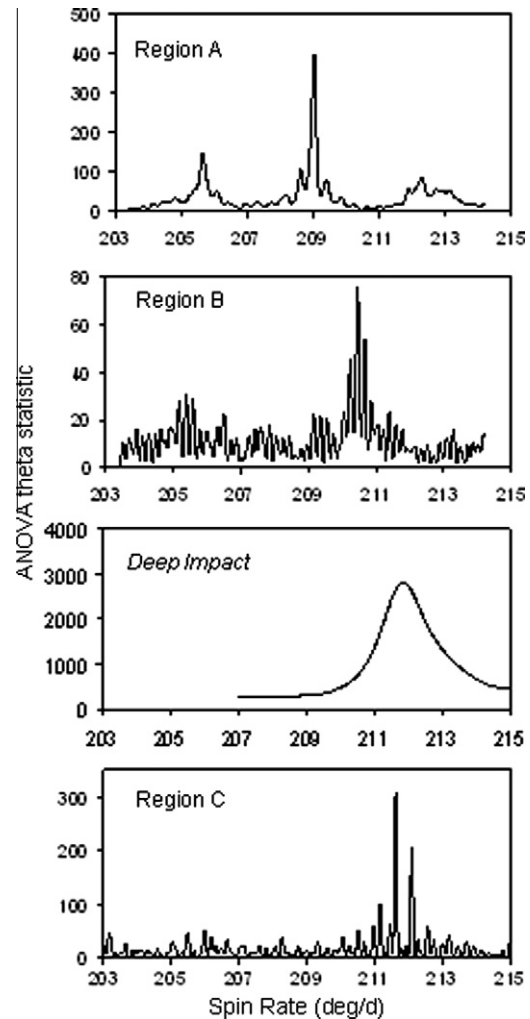


Fig. 15. ANOVA periodograms for the data in Figs. 9 and 11.

the JPL estimate without the careful bookkeeping and modification of the time tags required for the Tucson method. However, because of its reliance on the light curve generation tool, and in particular the Thomas et al. shape model, which did not accurately model the light curve at some rotation angles, the JPL approach suffered from somewhat poor fits. This led to some irresolvable ambiguities in determining which frequency was correct. In contrast, the Tucson approach did not rely on light curve models, or any other model, to identify the best fitting rotation rate. In this sense the Tucson approach is more robust in determining the rotation rate, while the JPL method seamlessly revealed the rotation phase of the comet.

6. The dynamical evolution of the spin rate of 9P/Tempel 1

Tables 2 and 3 contain our best estimates of the overall spin state of 9P/Tempel 1 and the changes that occurred during the perihelion passages in 2000 and 2005. Table 3 focuses on spin rates and orientation of the polar axis while Table 2 gives information on rotational phase. The spin rates and acceleration in Table 3 are the average of the values found in the JPL and Tucson studies.

In Fig. 18 we plot the observed spin rates and acceleration as a function of time. The spin rates derived from Earth-based measurements can be seen to systematically increase as the comet passes through succeeding perihelia in agreement with the sense, but not the slope, of acceleration that is derived from the *Deep Impact* photometry alone. Referring to the discussion in Section 4 we

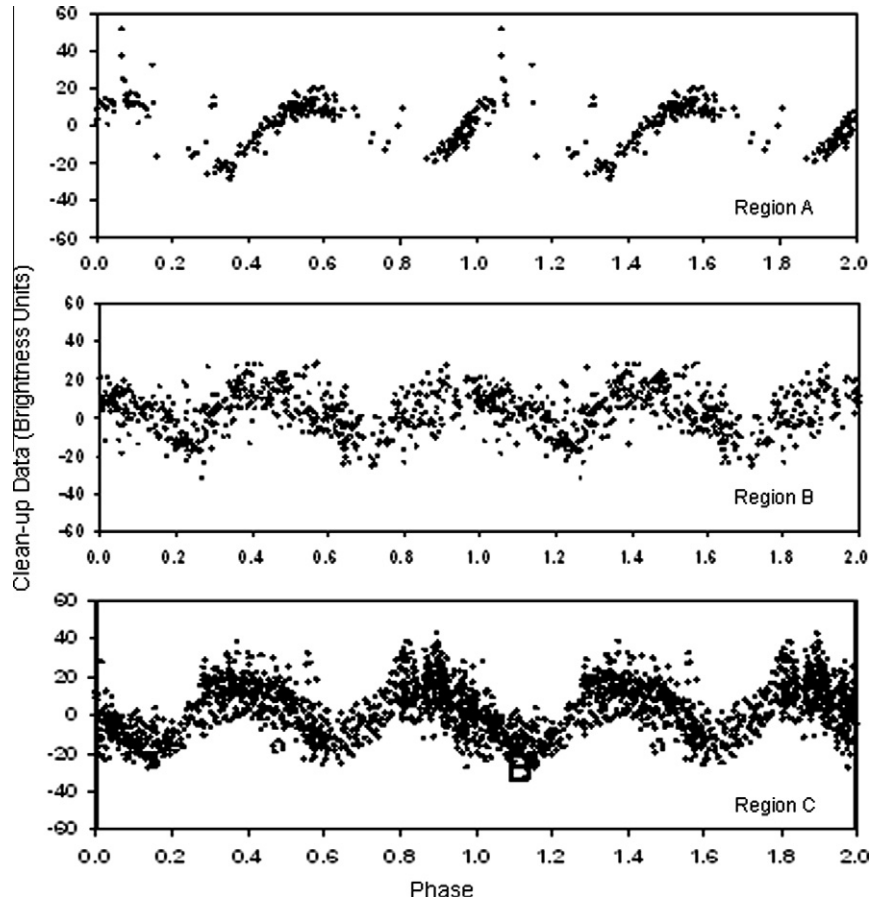


Fig. 16. The cleaned-up data for each observation region phased with the spin rates in Table 3.

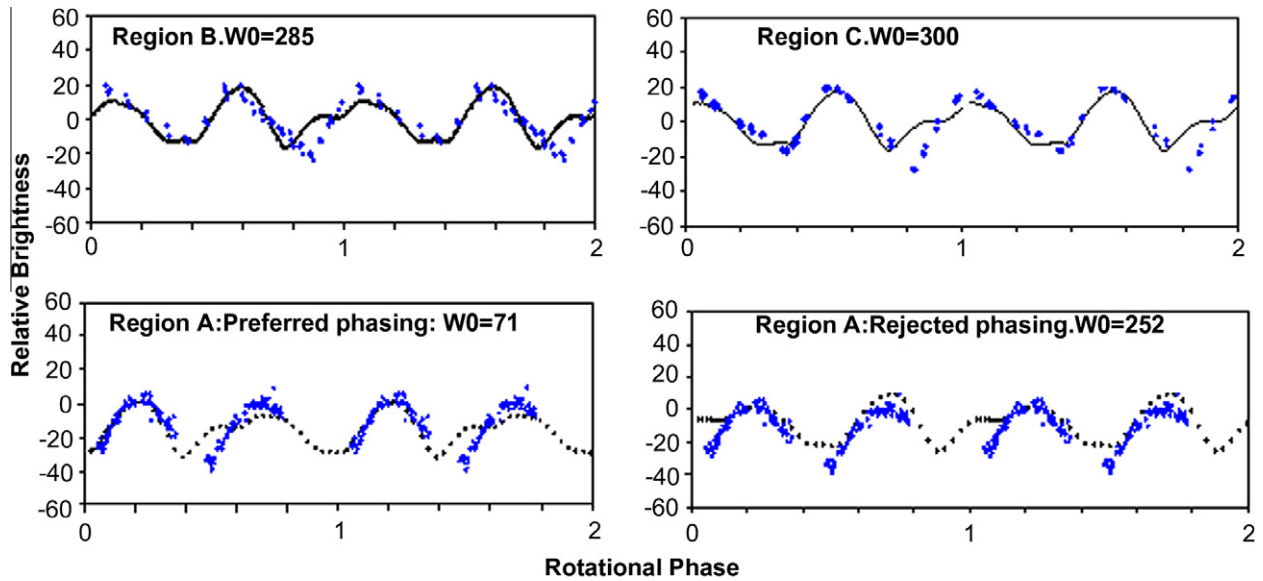


Fig. 17. Fits of model light curves to the *HST* data that determine the rotational phase in each observation region. In the top two panels we show the preferred fit based on numerical cross-correlation and visual inspection. Both of these methods give only marginal assurance of the best fit (i.e., a 180° ambiguity is possible). Note the discrepancy in the fit near the primary minimum in both sets of data. In the bottom two panels we show the fit of the model to a combination of Region A *HST* and ground-based data again illustrating the possibility of a 180° ambiguity.

assume that the changes in spin rate are the result of a smooth evolution of non-gravitational torques through perihelion and from perihelion to perihelion. The fact that the spin rate measured by

Deep Impact is greater than that measured both before and after perihelion and that it is closer in value to that measured after perihelion suggests that non-gravitational torques are not symmetric

Table 2

Results of rotational analysis: Values of $W(t_j) = W_{0j} + S_j * \Delta t$ for each region. Units: W_{0j} are in degrees, S_j are in $^{\circ}/\text{dy}$, and dS_{DI}/dt is in $^{\circ}/\text{dy}/\text{dy}$. $\Delta t = (t(\text{JD}) - 2451545.0)$. The spin rates for the *Deep Impact* data are given for the case of zero acceleration. When evaluating the values of W_{0j} between the two studies note that part of the difference is due errors in S_j propagating back to the reference time. The intrinsic lightcurve fitting error in $W_{0j}(\sim \pm 2^{\circ})$ is therefore much less than the differences would imply. Formal errors are given in the text.

JPL method	Tucson method
$W(t)_A = 67 + 209.023 \pm 0.004\Delta t$	$W(t)_A = 72 + 209.023 \pm 0.025\Delta t$
$W(t)_B = 289 + 210.438 \pm 0.001\Delta t$	$W(t)_B = 280 + 210.458 \pm 0.016\Delta t$
$W(t)_{DI} = 322 + 211.849 \pm 0.007\Delta t$	$W(t)_{DI} = 299 + 211.862 \pm 0.030\Delta t$
$W(t)_C = 299 + 211.626 \pm 0.001\Delta t$	$W(t)_C = 301 + 211.623 \pm 0.010\Delta t$
$dS_{DI}/dt = 0.024 - 0.028$	$dS_{DI}/dt = 0.020 \pm 0.003$

about perihelion and that, for a part of the time, positive torques dominate while at other times the reverse is true. It seems clear that the dominant effects of non-gravitational torques occur well before perihelion passage.

The acceleration measured during *Deep Impact* approach allows us to compute the magnitude of the torques acting on the nucleus at that time and estimate the moment arm that was involved. Assuming a homogeneous mass distribution in the interior, a

spherical approximation for the shape, and using the mass range determined by Richardson et al. (2007), we find that the moment of inertia of the nucleus lies between 0.8 and $4.6 \times 10^{19} \text{ kg m}^2$. To achieve the observed spin rate acceleration implies that a torque of $0.3\text{--}2.5 \times 10^7 \text{ kg m}^2 \text{ s}^{-2}$ was acting on the nucleus. Jewitt (1997) has related the average torque to total mass loss in terms of a “dimensionless moment arm,” k_T , for which he conjectured a value of ~ 0.05 . With the measurements reported here we can now make an *observational* estimate of k_T for 9P. Schleicher (2007) finds the production rate of OH to be $\sim 7 \times 10^{27} \text{ mol/s}$ near the relevant time implying a water loss rate of only $\sim 2 \times 10^2 \text{ kg/s}$. Following Jewitt (1997) we assume a characteristic outflow velocity of 10^3 m/s and find $0.005 < k_T < 0.04$. This observational estimate is somewhat lower than Jewitt’s conjecture but the result generally substantiates his approach.

The magnitude of the torque also permits us to say something about the stability of the pole direction. If we assume that there is a component of the torque acting at right angles to the spin axis for ~ 60 days (see Section 5 above) we can estimate the angular displacement under forced precession during this time. The angular velocity of precession calculated this way is $\sim 1 \times 10^{-9} \text{ rad s}^{-1}$ and leads to a displacement angle of $\sim 0.3^{\circ}$ during perihelion passage. Unless the observed torque turns out to be a very small

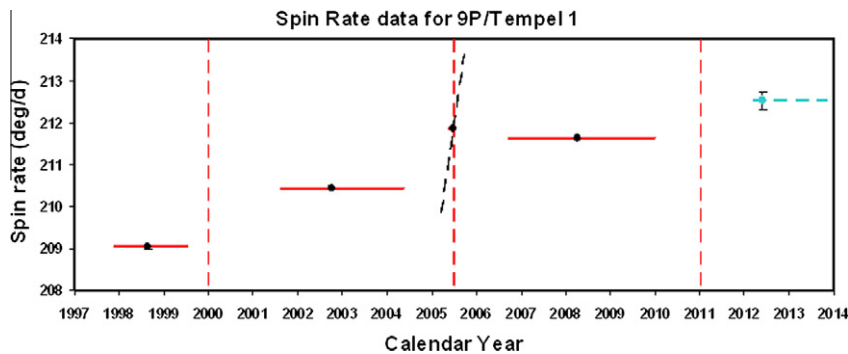


Fig. 18. Spin rate results for 9P/Tempel 1. The black points are the spin rates deduced from the data in Regions A, B, *Deep Impact*, and C and listed in Table 3. The black dashed line indicates the acceleration determined from the *Deep Impact* approach photometry. The horizontal red lines show the time period covered by the data in each region that was used to estimate the spin rate. The predicted spin rate ($212.522 \pm 0.174^{\circ}/\text{dy}$) near aphelion following the 2011 *Stardust-NEXT* encounter is shown in aqua. The observational error associated with the observed points is smaller than the dots; the error in the predicted point is a formal 1σ error based on an extrapolation from the observations taken around the 2000 and 2005 perihelia. The vertical dashed lines in red show where the perihelia of 2000, 2005 and 2011 fall.

Table 3

The observed spin state of 9P/Tempel 1 and its changes through two perihelion passages (in 2000 and 2005). *This estimate includes the effect of acceleration (assumed linear) during *Deep Impact* (DI) approach. + This estimate assumes zero acceleration in the spin rate during *Deep Impact* (DI) approach. Information on rotational phase is included in Table 2.

Orientation and sense of rotation		References		
Sense of spin	Direct	Thomas et al. (2007)		
Direction of pole (Positive or North)	RA = 294° , Dec = 73° ($\pm 5^{\circ}$ on the sky; J2000)	Thomas et al. (2007)		
Motion of the pole	Precession possible? Change not detected over eight apparitions. $< 1^{\circ}/\text{perihelion passage}$. Nucleus in essentially fully relaxed SAM (Short Axis Mode) state of rotation	Yeomans et al. (2004b), Schleicher (2007) and This paper		
Rotation rates	Epoch (days) (JD – 2450000)	Period (days)	Angular rate ($^{\circ}/\text{day}$)	
Pre-2000	1224.88	1.7223 ± 0.0002	209.023 ± 0.025	This paper
2001–2004	2477.37	1.7106 ± 0.0001	210.448 ± 0.016	This paper
<i>Deep Impact</i> Approach*	3530.60	1.6996 ± 0.0002	211.814 ± 0.029	This paper
<i>Deep Impact</i> Approach*	3544.50	1.6993 ± 0.0002	211.856 ± 0.030	This paper
Post-2005	4297.00	1.7011 ± 0.0001	211.625 ± 0.012	This paper
Rotational acceleration		dP/dt (days/day)	$d\omega/dt$ ($^{\circ}/\text{day}^2$)	
<i>Deep Impact</i> approach	3530.60	$-1.9 \pm 0.1 \times 10^{-4}$	0.024 ± 0.001	This paper
Net change in rotation		ΔP (min)	$\Delta\omega$ ($^{\circ}/\text{day}$)	
2000 perihelion passage	1546.13	-16.8 ± 0.3	1.425 ± 0.030	This paper
2005 perihelion passage	3556.82	-13.7 ± 0.2	1.177 ± 0.020	This paper

component of the total torque that is operating, which we think is unlikely, we expect that the pole direction of 9P/Tempel 1 should not precess more than $\sim 1^\circ$ per perihelion passage.

6.1. Modeling the evolution of the spin state

One of the objectives of this work is to predict the rotational state of the nucleus near the time of the *Stardust-NExT* encounter on February 14, 2011. To do this a model of the non-gravitational torques is required. We have taken two approaches to develop such models – a *physical* approach, in which we attempt to emulate what we know about the comet’s sublimation rates and jet structures, and an *analytic* approach that models the time behavior of torques with a prescribed functional form. As with the rotational analysis this modeling was done independently at both JPL and in Tucson with similar results.

Our physical modeling of torques was based on a heuristic ‘rotating jet’ model that has been used earlier to analyze the effects of non-gravitational forces on cometary orbits (Chesley and Yeoman, 2005) and in which the dependence of torque on heliocentric distance is prescribed by the function $g(r)$ (Marsden et al., 1973). This sublimation “law” has had wide use in non-gravitational force studies (Yeomans et al., 2004a). With this kind of model it is possible to match the spin rates and rotational phases of the nucleus across both the 2000 and 2005 perihelion passages; however, we also found that it was not possible to match the acceleration of the spin rate measured on *Deep Impact* approach at the same time. For this reason modeling based on jet torques was abandoned by both groups. An alternative physical approach is to consider torques associated with widespread sublimation of H_2O over the surface of the nucleus employing the Thomas et al. (2007) shape model. Such a study is already underway and early results indicate that model period changes through perihelion are somewhat similar to those measured in this work and that phases of both positive and negative net torque can occur during perihelion passage. Since this work was already in an advanced state we decided not to duplicate the effort and focused instead on analytic modeling. Since the analytic models produced at JPL and Tucson are quite different, we present them separately. Even though the methods used by the two groups are quite different we shall find that they yield very similar descriptions of how the net torques currently operate during perihelion passage: on approach the spin rate first decreases, passes through a minimum, and then accelerates rapidly through perihelion. After perihelion the spin rate goes through a maximum and then decreases to a stable level as the nucleus moves away from the Sun.

6.2. The JPL torque model

Given the solutions detailed in Table 2 we can try to link together the various quiescent periods by examining the rotation phase runoffs induced by the torques encountered during the active intervals. We start with the 2005 perihelion passage since this case affords information on the comet’s rotation state near the time of perihelion, as well as before and after. From fits to the *Deep Impact* approach data we know that the rotation phase $W = 219^\circ$ on 2005 July 5.0 at perihelion. Meanwhile the pre- and post-perihelion quiescent solutions (Regions B and C in Table 2) predict $W = 225^\circ$ and $W = 104^\circ$, respectively, at perihelion. These imply that the accelerated comet gained 354° or -6° in rotational phase as it approached relative to a hypothetical unaccelerated comet. We call this the runoff. Similarly, but working in reverse time, the post-perihelion runoff is 245° relative to the unaccelerated post-perihelion solution. Thus according to these estimates the combined pre- and post-perihelion runoff is 239° (modulo 360°).

Using a similar approach at the 2000 perihelion, but without any active period constraints, we find that the combined runoff should have been about 208° , again modulo 360° .

We could not identify a torque profile that meets all of the constraints and leads to 354° runoff at perihelion, while we have developed an *ad hoc* model that does lead to -6° runoff (Fig. 19). This model assumes piece-wise constant accelerations, and thus piece-wise linear spin rates. The key feature is that there is a modest (and so far not directly observed) deceleration before the dramatic acceleration seen in the *Deep Impact* data begins. This deceleration period would be about $-0.0013^\circ/\text{dy}^2$ and would start 400 days pre-perihelion and end 660 days post-perihelion, which corresponds well to the active periods seen in Fig. 4. Interrupting this background deceleration is a period of acceleration of approximately $0.029^\circ/\text{dy}^2$ that acts only for the 86 days before perihelion. This scheme would arise from a diffuse negative torque that acts for most of the active period and a single, strong, seasonal, jet-like active region that only acts for the three months prior to perihelion.

While this model is obviously crude and lacks a detailed physical basis, it does meet the observational constraints and serves one of the key purposes of the project, which is to predict the spin state of the comet at the epoch of the *Stardust-NExT* flyby in mid-February 2011. Here we can assume that the comet will essentially do the same as it did in 2005, or we can assume that there is some secular change and extrapolate from 2000 to 2005 to 2011. The former assumes implicitly that the perihelion-to-perihelion changes are best modeled as a random walk, while the latter would be most appropriate under the assumption that the comet is changing in a predictable way. Given the paucity of information we have about the variability of comet nucleus activity, each of these perspectives are equally defensible. For the present model we assume the random walk hypothesis and thus predict that the 2011 runoff will be -6° to perihelion (2011 January 12.4). The additional 33 days from perihelion to the *Stardust-NExT* encounter (about 2011 February 15) should accumulate an additional 55° of runoff, amounting to a total of roughly 49° . The quiescent, post-2005 solution predicts $W = 349^\circ$ at 2011 February 15. Adding in the presumed runoff of 49° yields the accelerated prediction, $W = 38^\circ$. The spin rate at that time should be $213.53^\circ/\text{dy}$ giving $W_0 = 172^\circ$ and, on 2011 February 15.0, the sub-solar longitude is calculated to be 328° . The mission target is $W = 98^\circ$ at closest approach, and so the flyby should be delayed by 60° , i.e., delay the encounter to 2011 February 15.28. This is a 10 h delay from the nominal (i.e., before February 2010) arrival time of 2011 February 14.8625.

6.3. The Tucson or “Gauss” analytic model

Here we divide the component net torque, $T(t)$, at time t in Eq. (5) into two parts, to give the model the flexibility to represent both negative torques and positive torques separately as follows:

$$T(t) = T_1 \exp((t - t_{max1})/\tau_1)^2 + T_2 \exp((t - t_{max2})/\tau_2)^2 \quad (10)$$

The Gaussian shape assumed here is quite arbitrary and was chosen simply because it had the right *general* character for torques generated by sublimation and, more importantly, it allowed the integration for the spin rate to converge. The shape should be thought of as an interpolation function. We did experiment with Lorentzian shapes, but found that the extended wings gave unrealistic torques that extended too far into the region around aphelion.

The model therefore has six parameters, T_1 , T_2 , t_{max1} , t_{max2} , τ_1 , and τ_2 and, when applied to the 2005 perihelion passage, seven constraints – the observed spin rate and rotational phase at three times and the acceleration of the spin rate at a single time. A *MathCad* program was developed to solve Eq. (6) as a function of as-

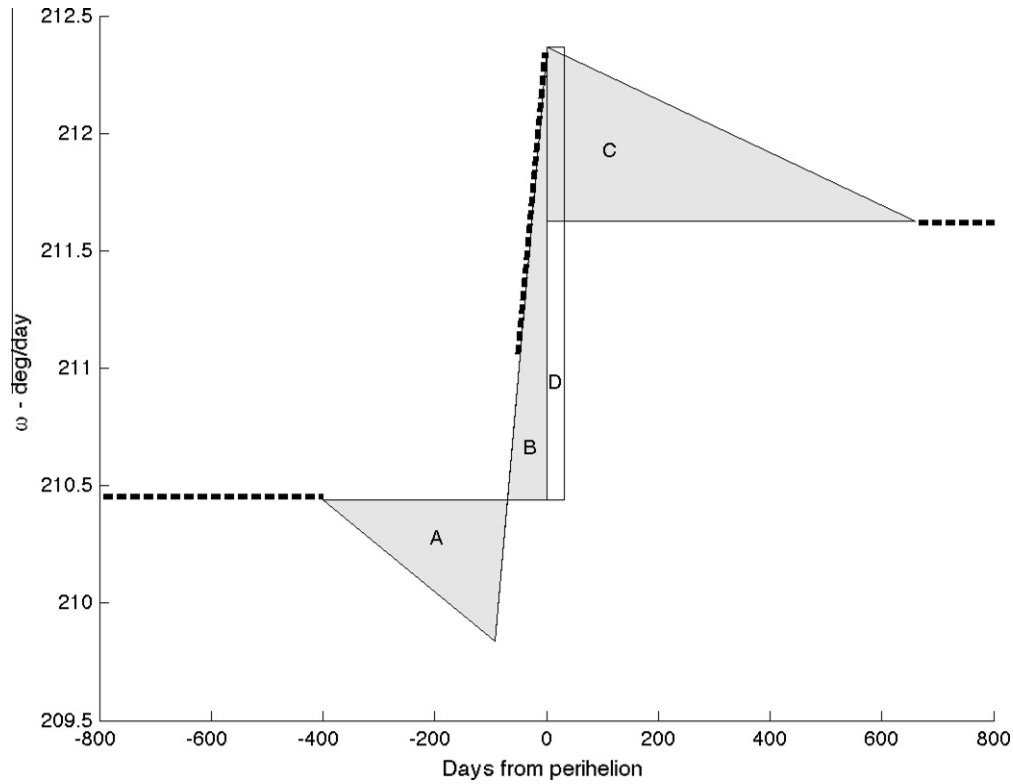


Fig. 19. JPL torque model. Bold dashed segments depict constraints obtained from photometric fits, before, during and after the 2005 perihelion passage. Area of triangles are $A = -74^\circ$, $B = 68^\circ$, $C = 245^\circ$. Area of rectangle D is $\sim 55^\circ$. Area $A + B + D = 49^\circ$ is the estimate of the rotation runoff from the pre-perihelion, quiescent solution (Region B) at the epoch 33 days after perihelion, which corresponds to the *Stardust-NExT* flyby.

sumed values for the parameters t_{max1} , τ_1 , and τ_2 . Preliminary values for T_1 , T_2 and t_{max2} were first estimated using the three observed spin rates and the acceleration at *Deep Impact* encounter. Given the initial rotational phase in a torque free region, Eq. (7) could then be integrated to provide an estimate of the rotational phase spin rate at the time of the other two observations. The parameters t_{max1} , τ_1 , and τ_2 were then adjusted in an iterative cycle until the model rotational phases agreed with the observed values to better than 1° .

At the 2000 perihelion we have only four constraints and it is not possible to solve for all of the parameters. We have therefore assumed that the parameters that depend primarily on the geometry of the perihelion passage, t_{max1} , t_{max2} , τ_1 , and τ_2 , have the same values as in 2005. We expect this to be a reasonable assumption provided that any precession of the spin pole (or the orbit) is, as we have assumed, negligible. In this way it is possible to calculate appropriate values of T_1 and T_2 for the 2000 perihelion passage.

The results of these calculations are collected in Table 4 and the torque profile and spin rate evolution for the 2005 perihelion passage are shown in Fig. 20. We see that the observations, as expected, require T_1 and T_2 to have opposite signs. The predicted net torque profile initially moves to a negative value before achieving a positive maximum some 32 days before perihelion. In addition, as expected from the decrease in the amount of period change through the 2005 perihelion relative to that at the 2000 perihelion, the magnitudes of the model torques are also seen to decrease from 2000 to 2005.

We use the parameters determined at the 2000 and 2005 perihelion passages to predict what the torque profiles may look like in the 2011 perihelion passage. First, we again assume that the parameters that depend primarily on geometry remain the same in 2011 as in 2005. Second we linearly extrapolate the values of T_1 and T_2 found in 2000 and 2005 to 2011. The resulting values

of the T_1 and T_2 are shown in Table 4, and the predicted spin rate profile for 2011 is plotted in Fig. 21. Putting these three solutions together we can plot our estimate for the complex evolution of the spin rate throughout the period 1997–2010 and the prediction for 2011. This is done in Fig. 22.

7. Discussion and predictions for Stardust-NExT encounter

The observations collected during the *Deep Impact* and *Stardust-NExT* international observing campaign cover an interval of thirteen years and two perihelion passages and clearly imply (Fig. 18) a roughly “stepwise” increase of the spin rate of 9P/Tempel 1 as the comet passes through succeeding perihelia. In addition, most of the torque must have been applied well before perihelion. The spin rate and its acceleration measured from the *Deep Impact* approach photometry imply even greater complexity in requiring that phases of both positive and negative net torque operate through the observed perihelion passages. The observations and modeling appear to support the idea that the torque producing outflow is dominated by the sublimation of H_2O over a large fraction of the surface of the nucleus and is a result of its shape. Modeling indicates that the production of net torque is unlikely to be

Table 4
Parameters for the Tucson “Gauss” torque model. The parameters are defined in Eq. (10). Details of the fitting process to the 2005 and 2000 perihelion spin rate and acceleration data is described in the text. The units of T_1 and T_2 are $^\circ/dy/dy$.

Perihelion	T_1	T_2	τ_1 (d)	τ_2 (d)	t_{max1} (d)	t_{max2} (d)
2000	-0.112612	0.132565	180	159	-16.9	-22
2005	-0.110612	0.129355	180	159	-16.9	-22
2011	-0.108612	0.126145	180	159	-16.9	-22

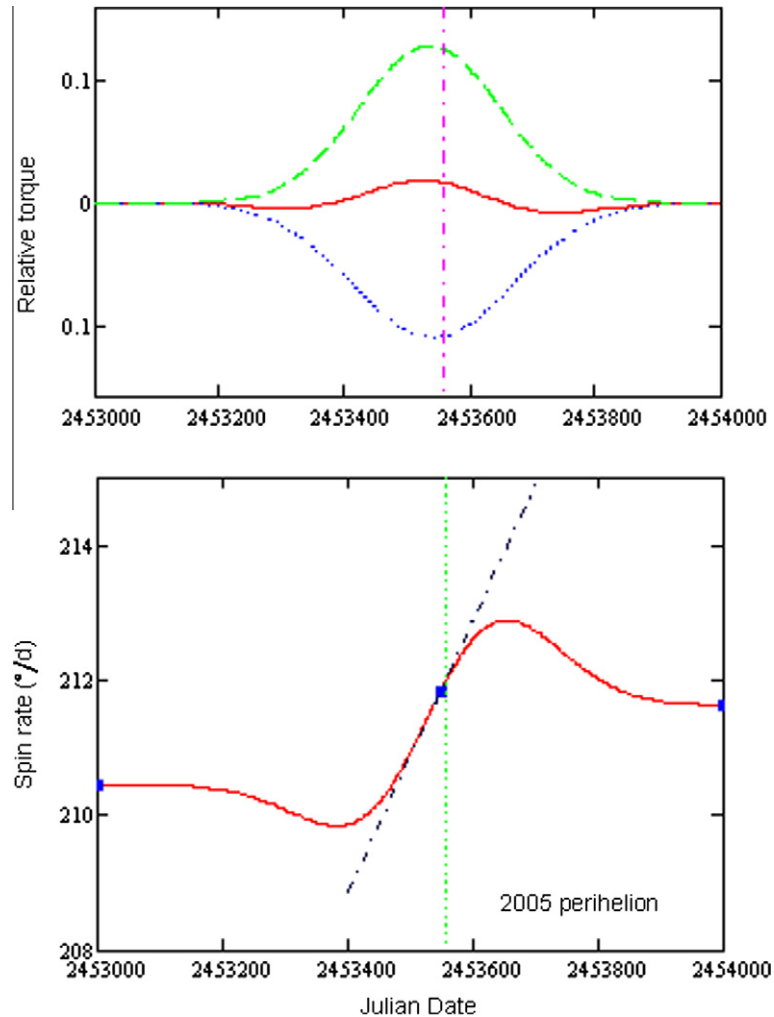


Fig. 20. Fit of the “Gauss” torque model to spin rate and rotational phase data spanning the 2005 perihelion and including the *Deep Impact* results. (*Top panel*) The component torques (green and blue) and the net torque (red) scaled to unit moment of inertia as a function of time. Note that the net torque is predicted to maximize 32 days before perihelion passage (red dot-dash vertical line). The net torque is at first negative and then rises to a positive maximum. The torque falls off becoming negative again before fading out. The bulk of the torque operates for ~ 300 days around perihelion. (*Bottom panel*) The modeled run of spin rate in the vicinity of perihelion. The observed spin rates are marked in blue and lie precisely on the model curve. In addition the rotational phase at each point is reproduced to within $\sim 1^\circ$. The rate of change of the spin rate measured from the *Deep Impact* approach photometry is shown as an inclined dot-dash line. In this model the predicted slope near perihelion is not precisely satisfied with the predicted value $\sim 10\%$ less than the measured value.

dominated by observed jet structures except, possibly, in the period just before perihelion passage. While the spin pole direction is certain to precess as a result of these torques, the rate is expected to be small, $< 1^\circ$ per perihelion passage. If it becomes possible to measure the displacement of the direction of the spin pole at the *Stardust-NExT* encounter in 2011 we should be able to deduce more about the distribution of the outflow with respect the surface of the Thomas et al. (2007) shape model.

7.1. Relationship to the water production rate

Observations of OH production by Osip et al. (1992), Schleicher (2007), and Cochran et al. (2009) and, in particular, their interpretation by Schleicher, indicate that the water production rate peaks 30–60 dy before perihelion and has moved closer to perihelion by 5–10 dy between the 1983 and 2005 perihelion passages. Apportioning this change equally among the intervening perihelia gives a shift of roughly 1–3 dy per perihelion. In addition, the production rate decreased by 42% between 1983 and 2005.

These changes are qualitatively consistent with the present observations in that the period change, and therefore the implied

production rate of the operating outflow, decreased between 2000 and 2005. Also the (model) torque peaks well before perihelion (32 dy) as does the observed H_2O production rate. The H_2O production rate implied by the model at the peak torque fell by 5% between 2000 and 2005.

Our observations and analytic modeling do not provide a quantitative explanation for the shift of the H_2O production peak by 1–3 dy per perihelion passage. But we presume that this is the result of small changes in the distribution of sublimation over the nucleus surface from perihelion to perihelion or, possibly, slow precession of the spin axis.

7.2. Predictions for the Stardust-NExT encounter with 9P/Tempel 1

The primary objective of the mission is to see what changes occurred on the regions of the surface previously imaged in the *Deep Impact* mission as a result of the activity during a single perihelion passage and, secondarily, to characterize the artificial crater formed by the impactor spacecraft. In January, 2010, when time-of-arrival trajectory maneuvers were being planned, the spacecraft was projected to arrive at the comet on UT 2011, February 14 at

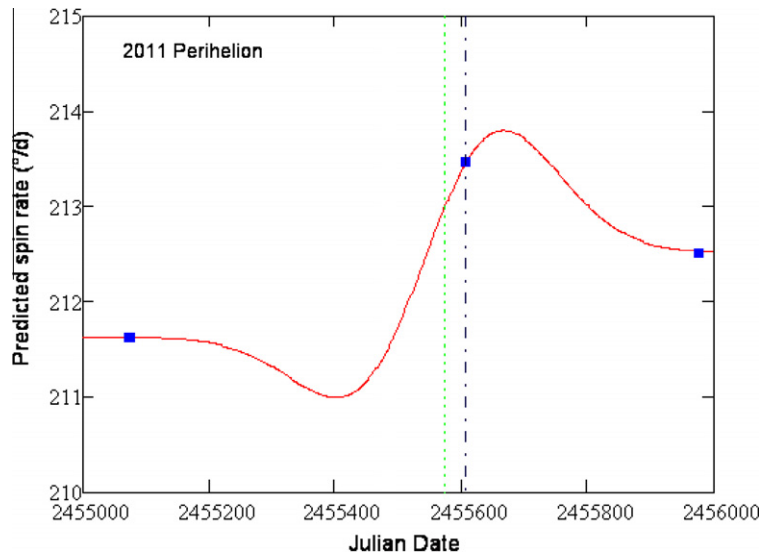


Fig. 21. The spin rates predicted by the “Gauss” model around the 2011 perihelion including the time of the *Stardust-NExT* encounter (February 14, 2011). The time of encounter is shown as a black dot-dash vertical line. The only measured spin rate in this figure is that at JD 2455074 the other two are predictions. The spin rate at encounter is estimated as $213.47^\circ/\text{dy}$. See text for details of the prediction. The time of perihelion is denoted with a vertical dotted green line.

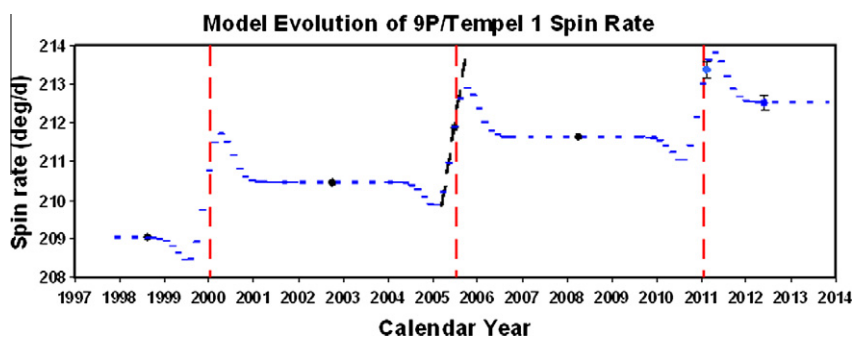


Fig. 22. Modeled evolution of the spin rate of 9P/Tempel 1 through three perihelion passages. The dashed blue line is the Gauss (see text), non-gravitational, torque model fit to the 2001–2004, *Deep Impact*, and post-2005 spin rates and rotational phases. The predicted evolution of the spin rate through the encounter of the *Stardust-NExT* mission on February 14, 2011, is also shown. The black points are the spin rates deduced from the data in Regions A, B, *Deep Impact*, and C that are listed in Table 2. The dashed line indicates the slope determined from the *Deep Impact* approach photometry. The predicted spin rates at encounter on February 14, 2011 ($213.47^\circ/\text{d}$) and near aphelion ($212.52^\circ/\text{dy}$) following the 2011 encounter are also shown. The vertical dashed lines in red show where the perihelia of 2000, 2005 and 2011 fall.

20:42:34.8 (JD 2455607.36290), some 34 dy after perihelion passage. To have the best chance of accomplishing these objectives the spacecraft should arrive at encounter when at least 25% of the *Deep Impact* observed regions and the crater are in daylight and visible to the spacecraft camera system. Fig. 23 is a contour plot that shows the encounter conditions that must prevail in order to achieve the above objectives. By providing a time-of-arrival (which sets the sub-solar longitude at encounter time) and a spacecraft B-plane angle that avoids the dark blue area it is possible to ensure that the mission will achieve its objective.

In the JPL study, in order to make a prediction for the spin state at *Stardust-NExT* encounter, the spin evolution model that was developed for the 2005 perihelion passage was simply transferred to the 2011 time frame by modifying the initial spin rate and rotational phase to that appropriate for region C. This approach was based on the assumption that changes in the torque profile from perihelion to perihelion cannot be easily predicted and that the comet is likely to behave at one perihelion essentially as it did at the previous perihelion. This yielded a spin rate of $213.52^\circ/\text{dy}$ and a sub-solar longitude of 328°W at encounter on UT 2011 Feb.15.0 (299°W on February 14 20:40).

In the Tucson study, the value of the parameters T_1 and T_2 in the Gauss model that are appropriate for the 2011 perihelion passage

are obtained by a linear extrapolation of their values in 2000 and 2005. The values of the other parameters in the Gauss model are, as explained earlier, taken to be the same as in 2005. The model yields a spin rate of $213.47^\circ/\text{dy}$, $W_0 = 15.9^\circ$, and a sub-solar longitude of 242°W on 2011 February 14 20:40. The two models differ by 57° in their prediction of sub-solar longitude. In order to be specific, and since the two results are reasonably close (i.e., both well within a single quadrant), we simply take their average as our final estimate for the sub-solar longitude at nominal encounter and treat the difference as an indicator of the level of uncertainty in the result, i.e., we take the sub-solar longitude at the nominal time of encounter (UT 2011 February 14 20:40) to be $271 \pm 29^\circ\text{W}$. This result is plotted on Fig. 23 as a black dot and bar and shows that a trajectory correction maneuver to delay the time-of-arrival by at least 8 h was needed to be sure of attaining the primary science objective. In Fig. 24 we show, using the Thomas et al. (2007) shape model, the predicted aspect of the nucleus as seen from the *Stardust-NExT* spacecraft at the nominal encounter time (LHS) and the case where the encounter time has been delayed by 8 h (RHS) where there is not only ample *Deep Impact* terrain to observe but also what should be a spectacular view of the artificial feature. A burn to accomplish a ~ 8 h delay in arrival time (the maximum allowed by the available fuel) was performed in February, 2010.

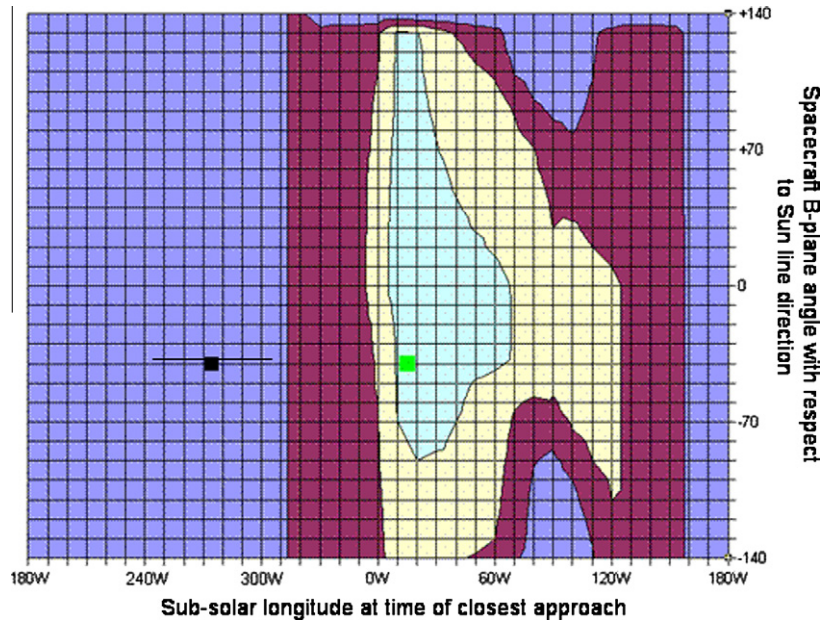


Fig. 23. Contour plot of the percentage of the 2005 *Deep Impact* imaging coverage that will be observable at *Stardust-NExT* encounter as a function of sub-solar longitude at the time-of-arrival and the spacecraft B-plane angle with respect to the sun-line. The B-plane includes the target and is orthogonal to the asymptotic approach velocity vector. The blue area is <25%, the magenta area achieves 25–50%, the yellow area achieves 50–75%, and the green area achieves 75–100%. The green dot denotes the arrival conditions for optimal viewing of the *Deep Impact* crater. The black dot and bar denotes the conditions for the nominal time-of-arrival on February 14, 2011 20:42 and its uncertainty given the predictions based on the observations analyzed here. Since it falls in the blue region of the plot, the Level 1 NASA requirement of imaging at least 25% of the *Deep Impact* coverage is unlikely to be attained without an adjustment of the time-of-arrival. A time-of-arrival adjustment with a delay of ~ 8 h is required to move the black point and its estimated error into the magenta area to achieve the requirement. Such an adjustment was made by a trajectory correction maneuver in February, 2010. (For interpretation of the references to color in this figure legend, the reader is referred to the web version of this article.)

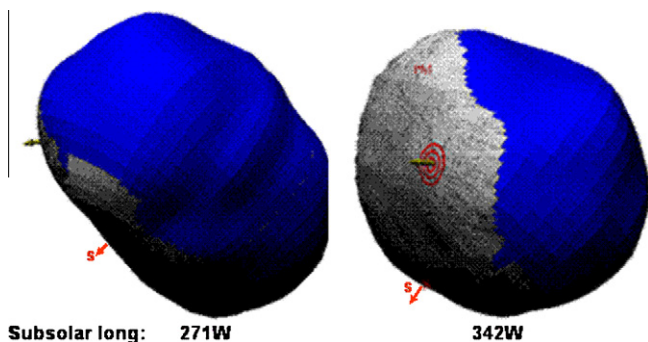


Fig. 24. The anticipated view of the nucleus of 9P/Tempel 1 from the *Stardust-NExT* spacecraft at closest approach on a trajectory that has the sub-spacecraft latitude at -11° . Grey represents areas previously imaged by *Deep Impact* while blue is *terra incognita*. Also shown is the position of the *Deep Impact* crater and the position of the South pole. The left panel shows the view with the nominal time-of-arrival in January 2010; the right panel shows the view with the recommended maximum 8 h delay in the time-of-arrival.

Finally, we note that there is an important caveat to the above prediction: there is, as noted in Section 5, the possibility of an error of 180° in the predicted rotational phase. If this is the case then the nominal encounter time will achieve excellent viewing of *Deep Impact* terrain at a sub-solar longitude of $\sim 91^\circ\text{W}$ without a trajectory correction maneuver. With a time delay of 8 h, implementing the trajectory correction moves the sub-solar longitude at encounter to $\sim 162 \pm 25^\circ\text{W}$. As can be seen from Fig. 23 this still allows the possibility that the primary science objective will be achieved, but that imaging of the artificial crater would be unlikely.

8. Conclusions

In this paper we have provided a detailed analysis of light curve information from the *Deep Impact* and *Stardust-NExT* international

observing campaign and data obtained from the *Hubble* and *Spitzer Space Telescopes* and the *Deep Impact* mission that were obtained between 1997 and 2009. This analysis shows:

1. The spin rate (period) changed in an approximately stepwise manner through the 2000 and 2005 perihelion passages, from $209.023 \pm 0.025^\circ/\text{dy}$ (1.7223 ± 0.0002 dy; 41.335 h) prior to 2000, to $210.448 \pm 0.016^\circ/\text{dy}$ (1.7106 ± 0.0001 dy; 41.054 h) between 2000 and 2005, then to $211.814 \pm 0.029^\circ/\text{dy}$ (1.6996 ± 0.0002 dy; 40.790 h) during the *Deep Impact* approach, and finally to $211.625 \pm 0.012^\circ/\text{dy}$ (1.7011 ± 0.0001 dy; 40.826 h) post-2005.
2. The period shortened by 16.8 ± 0.3 min during the 2000 perihelion passage and by 13.8 ± 0.2 min during the 2005 perihelion passage.
3. The angular acceleration was $0.024 \pm 0.003^\circ/\text{dy}^2$ during the *Deep Impact* approach.
4. In 2005 the angular acceleration was not symmetric about perihelion and most occurred well before perihelion passage.
5. Sublimation outflow of H_2O over most of the surface of the elongated nucleus with a possible contribution from jet activity just prior to perihelion are likely the causes of the torque.
6. The level of torque required to explain the *Deep Impact* observations suggests that precession of the spin axis is small, i.e., $<1^\circ$ per perihelion passage.
7. The trend in the net change of spin rate through the two perihelion passages is in the direction expected from the published trend in H_2O production rates observed at the 1983 through 2005 perihelia.
8. The observed peak in H_2O production rate some 30–60 days before perihelion is in concert with the predicted peak in torque at 32 days before perihelion. The H_2O production rate implied by the Tucson torque model fell by 5% between the 2000 and 2005 perihelia.

9. Analytic models have been used to predict the rotational state at the comet at the planned *Stardust-NExT* mission encounter in 2011. On UT February 14, 2011 20:40, the nominal encounter time, we predict that the sub-solar longitude on the nucleus will be $271 \pm 29^\circ$ West longitude (the average of the JPL (299° W) and Tucson (242° W) determinations). The spin rate is predicted to be $213.5 \pm 0.2^\circ/\text{d}$.

Acknowledgments

We thank J. Giorgini for assistance with the JPL Horizons system and Aron Wolff and the NExT navigation team for making available trajectory information of the *Stardust-NExT* spacecraft for the 2011 encounter with 9P/Tempel 1. We also thank D.K. Yeomans for insights into the non-gravitational force modeling. This research was performed with the University of Maryland under Contract NNM07AA99C, with Cornell University under agreement 51326-8361, and through a Grant, HST-GO-11998.03-A, awarded to the National Optical Astronomy Observatory (NOAO/KPNO) by the *Space Telescope Science Institute* operated by AURA. Belton Space Exploration Initiatives, LLC, is a sub-contractor to NOAO/KPNO and acknowledges their support.

This massive project, based on the data described in Meech et al. (2011, in press), would not have been possible without the support of observatory staff, support astronomers and the telescope operators. We would like to thank the UH2.2-m support staff who were a great help with the observations Lance Amano, Don De Cleene, John Dvorak, Paul Degrood, Chris Herrick, Chuck Sorenson, observers at the Purple Mountain Observatory Renquan Hong and Longfei Hu. We would also like to thank the observers who generously got an image of the comet for us, or a calibration field: Brian Barris (Northrup Grumman), Aaron Evans (University of Virginia), Chad Trujillo (Gemini Telescope), We especially thank Cedric Foellmi, science operations leader and Jorge Miranda the TO at La Silla, and Sangeeta Malhotra who took a few data points on the NTT 3.6-m and the CTIO 4-m telescopes in Chile on short notice when Mauna Kea closed during the Dec. 2003 blizzard. We thank Robert Gilmozzi, the Science Operations director at Paranal who awarded us the VLT time during January 2004. L.M. Lara acknowledges Chris Benn for acquiring some of the data and gratefully thanks him for observing when she became ill and could not observe. We especially thank Larry Wasserman for contributing data from several observing runs, and for his extensive help with set up and training at the Lowell 1.8 m telescope. We thank the staff of IAO, Hanle and CREST, Hosakote, that made these observations possible. The facilities at IAO and CREST are operated by the Indian Institute of Astrophysics, Bangalore.

This material is based upon work supported by the National Aeronautics and Space Administration through the NASA Astrobiology Institute under Cooperative Agreement No. NNA04CC08A issued through the Office of Space Science, by NASA Grant Nos. NAGW 5015, NAG5-4495, NNX07A044G, NNX07AF79G, NASA STScI HST-GO-11887.01A, Cornell subcontract 51326-8653 (*Stardust-NExT*), and through the US-Israel Bi-national foundation (BSF) and by the Israel Ministry of Science, through the Israel Space Agency. JP was supported, in part, by the Scientific Grant Agency VEGA of the Slovak Academy of Science, 2/7040/27. J. Licandro thanks funding from the National Plan of I+D+i project AYA2008-06202-C03-02 of the Spanish Ministry of Science and Innovation. B.E.A. Mueller, N. Samarasinha and T. Farnham were supported by NASA Grant NNG06G141G. This is PSI contribution 497. H. Zhao acknowledges the support by the National Natural Science Foundation of China (Grant Nos. 1050313 and 10933004) and the Minor Plant Foundation of Purple Mountain Observatory. Support for H. Hsieh was provided through STFC Fellowship Grant ST/F011016/

1, and by NASA through Hubble Fellowship Grant HST-HF-51274.01A awarded by the Space Telescope Science Institute, which is operated by the Association of Universities for Research in Astronomy, Inc., for NASA, under Contract NAS 5-26555.

This work is also based in part on observations obtained at the Gemini Observatory, which is operated by the Association of Universities for Research in Astronomy, Inc., under a cooperative agreement with the NSF on behalf of the Gemini partnership: the National Science Foundation (United States), the Science and Technology Facilities Council (United Kingdom), the National Research Council (Canada), CONICYT (Chile), the Australian Research Council (Australia), Ministrio da Cincia e Tecnologia (Brazil) and SECYT (Argentina).

The data are also based in part on observations obtained at the La Silla Paranal observatory of the European Southern Observatory, ESO. Telescope time was granted at Lowell Observatory through the PREST program, NSF Grant NSF04-557. This paper includes data taken at The McDonald Observatory of The University of Texas at Austin. This work is based in part on observations made with the WHT operated on the island of La Palma by the Isaac Newton Group in the Spanish Observatorio del Roque de los Muchachos of the Instituto de Astrofisica de Canarias. This work is based in part on observations obtained at the La Silla – Paranal observatory of the European Southern Observatory ESO in Chile. Data were obtained in part from the Liverpool Telescope which is operated on the island of La Palma by Liverpool John Moores University in the Spanish Observatorio del Roque de los Muchachos of the Instituto de Astrofisica de Canarias with financial support from the UK Science and Technology Facilities Council.

Appendix A. Description of the *Deep Impact* MRI photometric reductions (contributed by Fabienne A. Bastien)

Photometric measurements of comet 9P/Tempel 1 were performed on images taken with the Medium Resolution Instrument on the *Deep Impact* spacecraft during the approach phase from 1 May 2005 to ~6 h before impact on 4 July 2005. The MRI is a 12 cm aperture Cassegrain telescope with a 2.1 m focal length. Images were taken through clear filters that have a center wavelength of 650 nm and are uncoated and not band limited (Hampton et al., 2005).

A total of 3014 images were analyzed: 595 science images and 2419 optical navigation images. The measurements were based on circular apertures ranging from 5 to 30 pixels in diameter with the nucleus at the center of the aperture. The data consist of science images taken with the clear 1 and clear 6 filters and optical navigation images taken with the clear 1 filter. In the following discussion the images are displayed with lines increasing up and with samples to the right. Fig. A1 (taken from Klaasen et al., 2008) shows a full frame image with the quadrant nomenclature used below.

A.1. Properties of the science data

Photometric measurements were made from the reversibly calibrated (“RADREV”) science images. These images have had the standard pipeline corrections applied to them: bias and dark frame subtraction, flat-field corrections, etc. They have not, however, been “cleaned” to remove artifacts such as cosmic rays. All images were taken in one of two sub-frame modes: 256×256 pixels for most of the approach sequence, and 512×512 pixels for the last 1.7 days of approach. The images display a number of problems not accounted for in the standard reduction. All images were affected by a variable horizontal striping of a few DN in amplitude caused by electrical interference. Additionally, the bias levels for these images are only known to the nearest full DN, and the bias

level for each quadrant is different. Not correcting the images for this interference and, more importantly, for the imprecise bias subtraction can introduce systematic errors in the photometry by which the early approach images are primarily affected.

A further problem concerns the pixels in the two rows surrounding the horizontal boundary between the upper and lower halves of the CCD that are each $1/6$ of a pixel smaller than the other pixels of the CCD due to the way the readout clocking was designed. This feature increases the apparent point spread function of objects that overlap this boundary by $1/3$ of a pixel in the reconstructed images (which have uniform spacing). Flux measurements therefore tend to be greater at the boundary because the flat fielding during the pipeline processing designed to produce correct scene radiances for spatially resolved objects. In approximately 80% of the images, the centroid of the nucleus lies within 20 pixels of this region; images taken through the clear 6 filter are particularly affected. Thus, most of the photometric measurements need to be corrected for this effect.

A.2. Properties of the navigation data

The raw optical navigation images are in a different format from the science images. Each image consists of a number of square “snippets”, each less than 400×400 pixels in size. Each “snippet” is centered on an object deemed interesting by the navigation team, usually a star or 9P/Tempel 1. Each set of snippets is integrated into a single image that is 1008×1008 pixels in size; the navigation data have neither serial-overclock nor parallel-overclock pixels. Therefore, quadrant bias must be determined via other methods. For a more detailed description of the navigation data, please see the *Deep Impact* Navigation Images Report included in the *Deep Impact* documentation data set, DI-C-HR11/HR1V/MRI/ITS-6-DOC-SET-V1.0, which is archived by the Planetary Data System.

Optical navigation data suffer from the same striping noise as the science data. However, because these data are in a different format from the science data, a different algorithm had to be applied to correct it. This procedure was also used to remove the bias. For the navigation data, the centroid position of the comet was sufficiently far away from the horizontal boundary between the upper

and lower halves of the CCD (more than 30 pixels, on average) so that the photometric measurements were not affected by the smaller size of the pixels there.

A.3. Photometric reduction of the science data

The general procedure for the analysis of the science data is as follows: We start with RADREV calibrated data and then remove the horizontal striping. In order to remove the horizontal striping, the image is first divided into two halves: quadrants B and D to one side and quadrants A and C to the other. The process is similar for each half: a region is defined, avoiding the overclock pixels, which will be used to determine the background. This is a two-dimensional array 25 pixels wide and whose length depends on the size of the image (256 pixels or 512 pixels). We take a resistant mean across each row of this array and store into a new array that is 1 pixel wide and 256 pixels or 512 pixels long. This array is then subtracted from each column of the half-image. This process is illustrated in Fig. A2.

Once the background noise is removed, we then convert the data back to DN/s, and circular aperture photometry is performed with apertures ranging in size from 5 pixels to 30 pixels in diameter. If the aperture falls across the boundary between the upper and lower halves of the CCD, the following procedure is used to correct the flux: we create a sub-image centered on the comet that is slightly larger than the aperture. This sub-image is then divided into two parts: part 1 is the portion of the image located above the quadrant boundary and part 2 corresponds to the part below the boundary. We measure the flux contained within the original aperture (i.e. with the center of the aperture at the original centroid position) that is in part 1. The centroid of the aperture is then shifted up by $1/6$ of a pixel, and the flux re-measured. The difference between these two measurements is half of the necessary correction to be added to the total flux. The procedure is repeated for part 2, only this time the centroid of the aperture is shifted down by $1/6$ of a pixel. Finally, we take the two central rows of the CCD (rows 511 and 512), and measure the flux from these two rows that is contained within the aperture. One third of this value is subtracted from the total flux. Fig. A3 illustrates this procedure.

A.4. Photometric reduction of the navigation data

The process is similar to that used for the science images except that the correction for the quadrant boundary is not applied. The background removal algorithm that we apply to the navigation images differs from that used for the science images in that the edge of the relevant snippet is used to estimate the background instead of the edge of the image. Since the apertures used do not cross quadrant boundaries, it is only necessary to use one edge of the snippet. This procedure simultaneously determines the value of the background in the snippet and the bias.

Unfortunately this procedure does not work for images that were taken during the last week of approach. At this point, the comet’s coma contaminates the entire snippet centered on the comet, and rarely are there any other snippets within the same quadrant (this is always quadrant D during this time period). In this case the value of the background is measured from the raw science images taken closest in time to the navigation image under consideration. A slightly different bias value is subtracted from the navigation images (358.5 DN) than from the science images (359 DN); however since the bias values applied to the science data are only determined to the nearest full DN, these two numbers are consistent with one another. Note that horizontal striping is not removed from images taken during this time frame. At this point in the sequence the comet is bright en-

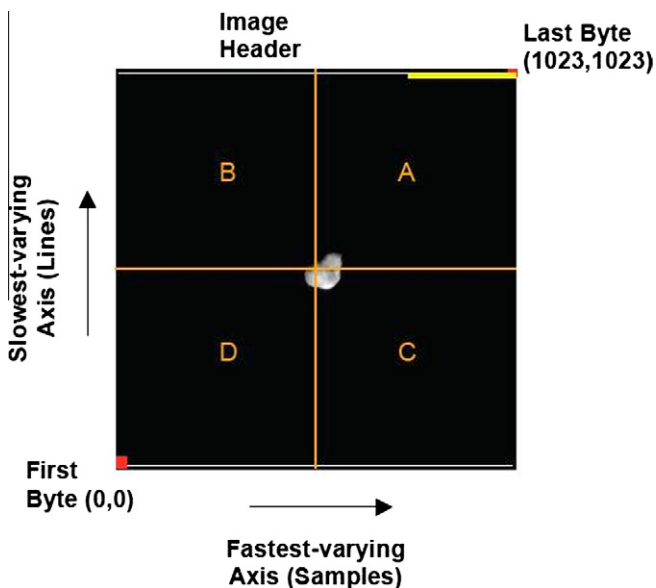


Fig. A1. A full frame MRI image showing the quadrant nomenclature.

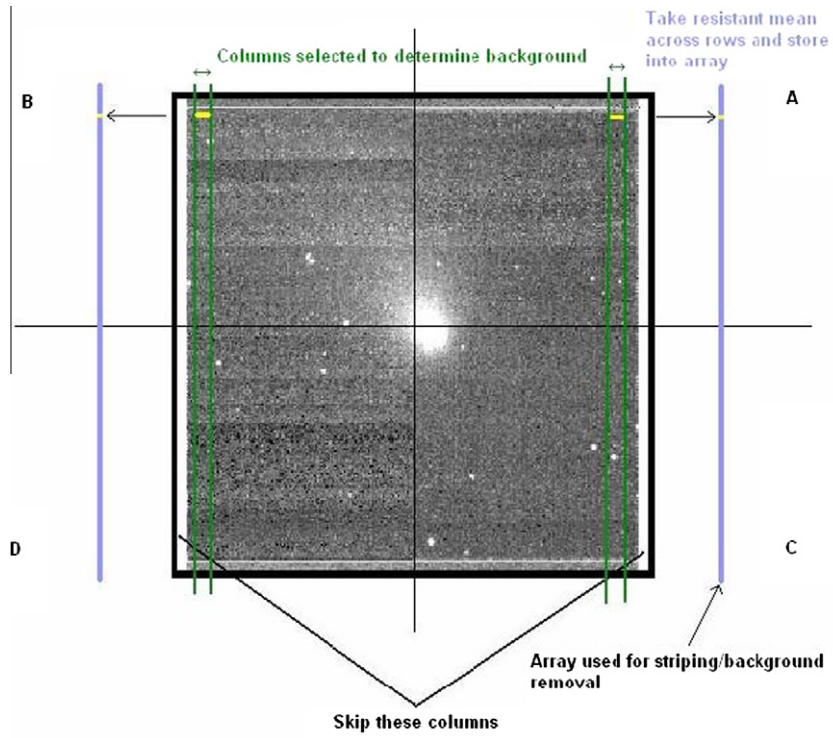


Fig. A2. Illustration of the procedure used to create a uniform background in the MRI science images.

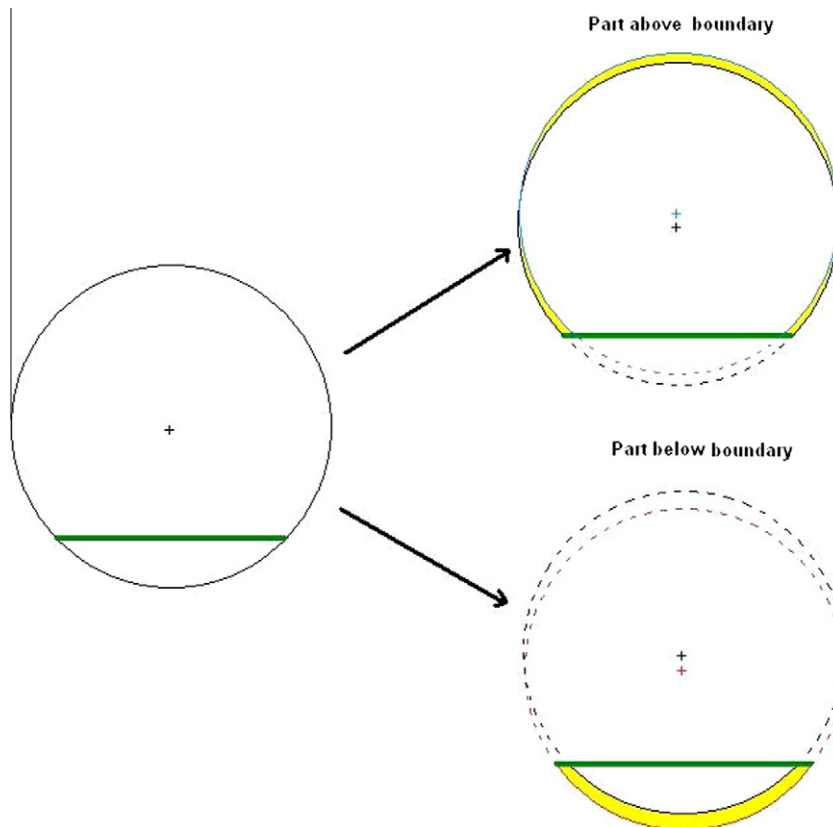


Fig. A3. Procedure used to correct comet flux measurements for the quadrant boundary effect (see text). The cross at the center of the aperture corresponds to the comet's centroid position. The green line represents the quadrant boundary. The correction consists of subtracting 1/3 of the flux from the rows at the boundary. The yellow shaded areas illustrate what is added back in.

ough for the effect to be negligible. In 12 cases the comet was close enough to the quadrant boundary to require correction to the flux. Since these images comprise less than 0.5% of the total number of navigation images, these data were simply omitted from the analysis.

Appendix B. Investigation of Deep Impact photometry with the dynamical techniques. Contributed by Michal Drahus

Deep Impact approach photometry (Section 3) was obtained close to perihelion, when the comet was active – thus providing an opportunity to seek angular acceleration in this data set alone. This acceleration would manifest itself as a small deviation from the constant periodicity. We performed such an analysis using the dynamical techniques introduced by Drahus and Waniak (2006).

We used their dynamical implementations of two classical algorithms: the Phase Dispersion Minimization (PDM), introduced by Stellingwerf (1978) and later improved by Drahus and Waniak (2006) to weight input data points according to their errors (which they called DPDM), and a Least Squares fit (hereafter harmonics fit) of a sum of harmonics, which also weights the input data. Both methods return a variance ratio R , which is a function of the rotation frequency ω_0 and acceleration $d\omega/dt$, and whose minima indicate the best dynamical solutions. Although the techniques allow for any *a priori* law controlling the accelerating torque, in our analysis we assumed it was constant. This implies a constant $d\omega/dt$ and a linear evolution of ω with time. When the frequency is labelled with index zero, it refers to a specific moment of time t_0 ; throughout this section t_0 is the middle moment of the DI data set, which is June 9, 2005, 2:31:20.6 UT (JD 2453530.60510).

Discovery of the secular spin-up of Tempel 1 made it possible to predict the frequency ω_0 and acceleration $d\omega/dt$ for the moment t_0 , and consequently to limit our analysis to the vicinity of the expected solution. Hence we investigated ω_0 between 0.024 and 0.025 h^{-1} (which corresponds to the periods P_0 between 1.667 dy [40.01 h] and 1.736 dy [41.66 h]), and $d\omega/dt$ between -5.0 and $+5.0 \times 10^{-7} \text{h}^{-2}$. The DPDM was used with 20–200 bins (and always five covers), and the harmonics fit with 3–7 harmonics (including the base sinusoid). However, the results were found to be very weakly dependent on the settings. For the sake of clarity we present the solutions from the DPDM with 60 bins and from the harmonics fit with five harmonics (Fig. B1), and adopt their mean value as the final dynamical solution.

The solution is $\omega_0 = 0.0245155 \pm 0.0000033 \text{h}^{-1}$ ($P_0 = 1.69961 \pm 0.00023$ dy; 40.791 h) and $d\omega/dt = +0.97 \pm 0.15 \times 10^{-7} \text{h}^{-2}$, which unambiguously confirms slow spin-up of the nucleus. The parameters are significantly correlated, with the correlation coefficient of -0.70 , which is a consequence of non-uniform distribution of the input data points. Note, that although data phasing is influenced simultaneously by ω_0 and $d\omega/dt$, for uniformly distributed points analysed with respect to the middle moment t_0 , the correlation would be weak or completely removed.

Errors and the correlation coefficient were estimated following the Monte-Carlo approach of Drahus and Waniak (2006). We take as the noiseless reference light curve the harmonics fit with five harmonics, calculated separately for the solutions from both methods. We simulated 1000 realizations of noise for each of them, and determined the covariance matrices. Consequently, the mean matrix provided the errors and the correlation coefficient for the mean solution. It is worth noticing, that the dispersion of both individual solutions about the mean is only 15% of the error in frequency and 56% of the error in acceleration, which shows an excellent consistency of both algorithms and suggests that uncertainties are reliably estimated.

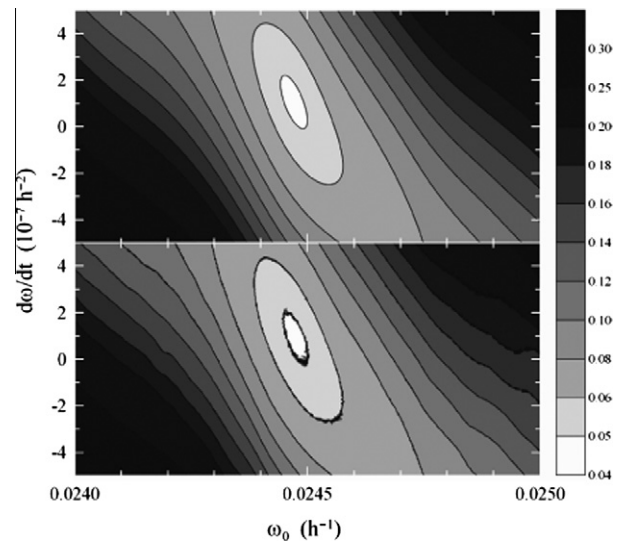


Fig. B1. Dynamical periodograms calculated with the methods of Drahus and Waniak (2006) showing the variance, R , in the Deep Impact approach photometry for assumed values of the spin rate and the spin rate slope. The Top Panel shows a harmonics fit with five harmonics, and the Bottom Panel shows the fit using the DPDM with 60 bins and five covers. The grey scale to the right indicates the range of R . Note that in both cases the minimum variance falls well above $d\omega/dt = 0$.

References

- A'Hearn, M.F. et al., 2005. Deep Impact: Excavating Comet Tempel 1. *Science* 310, 258–264.
- Asphaug, E., Benz, W., 1996. Size, density, and structure of Comet Shoemaker-Levy 9 inferred from the physics of tidal breakup. *Icarus* 121, 225–248.
- Belton, M.J.S., Gandhi, A., 1988. Application of the CLEAN algorithm to cometary light curves. *Bull. Am. Astron. Soc.* 20, 836.
- Belton, M.J.S., Melosh, H.J., 2009. Fluidization and multiphase transport of particulate cometary material as an explanation of the smooth terrains and repetitive outbursts on 9P/Tempel 1. *Icarus* 200, 280–291.
- Belton, M.J.S., Julian, W.H., Anderson, A.J., Mueller, B.E.A., 1991. The spin state and homogeneity of Comet Halley's nucleus. *Icarus* 95, 183–193.
- Belton, M.J.S. et al., 2005a. Deep Impact: Working properties for the target nucleus – Comet 9P/Tempel 1. *Space Sci. Rev.* 117, 137–160.
- Belton, M.J.S., Fernandez, Y.R., Samarasinha, N.H., Meech, K.J., 2005b. The excited spin state of Comet 2P/Encke. *Icarus* 175, 181–193.
- Belton, M.J.S., Thomas, P.C., Carcich, B., Crockett, C.J., 2006. The spin state of 9P/Tempel 1. *Lunar Planet. Sci.* 37, Abstract 1487.
- Belton, M.J.S., Feldman, P.D., A'Hearn, M.F., 2008. Cometary cryo-volcanism: Source regions and a model for the UT 2005 June 14 and other mini-outbursts on Comet 9P/Tempel 1. *Icarus* 198, 189–207.
- Brownlee, D.E. et al., 2004. Surface of young Jupiter family Comet 81P/Wild 2: View from the stardust spacecraft. *Science* 304, 1764–1769.
- Chesley, S.R., Yeoman, D.K., 2005. Nongravitational accelerations on comets. In: Knežević, Z., Milani, A. (Eds.), *Proc. IAU Colloq. #197, Dynamics of Populations of Planetary Systems*, pp. 289–302.
- Cochran, A.L., Barker, E.S., Caballero, M.D., György-Ries, J., 2009. Placing the Deep Impact mission into context: Two decades of observations of 9P/Tempel 1 from McDonald Observatory. *Icarus* 199, 119–128.
- Drahus, M., Waniak, W., 2006. Non-constant rotation period of Comet C/2001 K5 (LINEAR). *Icarus* 185, 544–557.
- Farnham, T.L. et al., 2007. Dust coma morphology in the Deep Impact images of Comet 9P/Tempel 1. *Icarus* 187, 26–40.
- Gutiérrez, P.J., Davidsson, B.J.R., 2007. Non-gravitational force modeling of Comet 81P/Wild 2: II. Rotational evolution. *Icarus* 191, 651–664.
- Gutiérrez, P.J., Ortiz, J.L., Rodrigo, R., López-Moreno, J.J., Jorda, L., 2002. Evolution of the rotational state of irregular cometary nuclei. *Earth Moon Planets* 90, 239–247.
- Gutiérrez, P.J., de León, J., Jorda, L., Licandro, J., Lara, L.M., Lamy, P., 2003. New spin period determination for Comet 6P/d'Arrest. *Astron. Astrophys.* 407, L37–L40.
- Hampton, D.L., Baer, J.W., Huisjen, M.A., Varner, C.C., Delamere, A., Wellnitz, D.D., A'Hearn, M.F., Klaasen, K.P., 2005. An overview of the instrument suite for the Deep Impact mission. *Space Sci. Rev.* 117, 43–93.
- Harris, A.W., Young, J.W., Scaltriti, F., Zappala, V., 1984. Lightcurves and phase relations of the Asteroids 82 Alkeme and 444 Gyptis. *Icarus* 57, 251–258.
- Harris, A.W. et al., 1989. Photoelectric observations of Asteroids 3, 24, 60, 261, and 863. *Icarus* 77, 171–186.
- Jewitt, D., 1997. Cometary rotation: An overview. *Earth Moon Planets* 79, 35–53.
- Jewitt, D., 2004. From cradle to grave: The rise and demise of the comets. In: Festou, M.C., Keller, H.U., Weaver, H.A. (Eds.), *Comets II*. University of Arizona Press, Tucson, pp. 659–676.

- Jorda, L., Gutiérrez, P.J., 2002. Rotational properties of cometary nuclei. *Earth Moon Planets* 89, 135–160.
- Klaasen, K.P. et al., 2008. *Deep Impact* instrument calibration. *Rev. Sci. Instrum.* 79, 1–77.
- Lamy, P., Toth, I., A'Hearn, M.F., Weaver, H., Weissman, P.R., 2001. Hubble Space Telescope observations of the nucleus of Comet 9P/Tempel 1. *Icarus* 154, 337–344.
- Lamy, P.L., Toth, I., A'Hearn, M.F., Weaver, H.A., Jorda, L., 2007. Hubble Space Telescope observations of Comet 9P/Tempel 1 during the *Deep Impact* encounter. *Icarus* 187, 113–122.
- Li, Jang-Yang et al., 2007. *Deep Impact* photometry of Comet 9P/Tempel 1. *Icarus* 187, 41–55.
- Lisse, C.M., A'Hearn, M.F., Groussin, O., Fernández, Y.R., Belton, M.J.S., van Cleve, J.E., Charmandaris, V., Meech, K.J., McGleam, C., 2005. Rotationally resolved 8–35 micron Spitzer Space Telescope observations of the nucleus of Comet 9P/Tempel 1. *Astrophys. J.* 625, L139–L142.
- Marsden, B.G., Sekanina, Z., Yeomans, D.K., 1973. Comets and nongravitational forces. *V. Astron. J.* 78, 211–225.
- Meech, K.J., Belton, M.J.S., Mueller, B.E.A., Dicksion, M.W., Li, H.R., 1993. Nucleus properties of P/Schwassmann-Wachmann 1. *Astron. J.* 106, 1222–1236.
- Meech, K.J. et al., 2005. *Deep Impact*: Observations from a worldwide Earth-based campaign. *Science* 310, 265–269.
- Meech, K.J., Pittichová, J., Yang, B., Zenn, A., Belton, M.J.S., A'Hearn, M.F., Bagnulo, S., Bai, J., Barrera, L., Bauer, J.M., Bedient, J., Bhatt, B.C., Boehnhardt, H., Brosch, N., Buie, M., Candia, P., Chen, W.-P., Chesley, S., Chiang, P., Choi, Y.-J. et al., 2011. *Deep Impact*, Stardust-NExT and the Behavior of Comet 9P/Tempel 1 From 1997–2010, *Icarus*, in press.
- Mueller, B.E.A., Ferrin, I., 1996. Change in the rotational period of Comet P/Tempel 2 between the 1988 and 1994 apparitions. *Icarus* 123, 463–477.
- Osip, D.J., Schleicher, D.G., Millis, R.L., 1992. Comets: Ground-based observations of spacecraft mission candidates. *Icarus* 98, 115–124.
- Richardson, J.E., Melosh, H.J., Lisse, C.M., Carcich, B., 2007. A ballistics analysis of the *Deep Impact* ejecta plume: Determining Comet Tempel 1's gravity, mass, and density. *Icarus* 190, 357–390.
- Rutherford, D.E., 1951. *Classical Mechanics*. Oliver and Boyd, Edinburgh and London.
- Samarasinha, N.H., A'Hearn, M.J., 1991. Observational and observational constraints on the rotation of Comet P/Halley. *Icarus* 93, 194–225.
- Samarasinha, N.H., Belton, M.J.S., 1995. Evolution of rotational states and non-gravitational effects for Halley-like cometary nuclei. *Icarus* 116, 340–358.
- Samarasinha, N.H., Mueller, B.E.A., Belton, M.J.S., Jorda, L., 2004. Rotation of Cometary Nuclei. In: Festou, M.C., Keller, H.U., Weaver, H.A. (Eds.), *Comets II*. University of Arizona Press, Tucson, pp. 281–299.
- Schleicher, D.G., 2007. *Deep Impact*'s target Comet 9P/Tempel 1 at multiple apparitions: Seasonal and secular variations in gas and dust production. *Icarus* 191, 322–338.
- Schleicher, D.G., Barns, K.L., Baugh, N.F., 2006. Photometry and imaging results for Comet 9P/Tempel 1 and *Deep Impact*: Gas production rates, post impact light curves, and ejecta plume morphology. *Astron. J.* 131, 1130–1137.
- Schwarzenberg-Czerny, A., 1991. Accuracy of period determination. *Mon. Not. R. Astron. Soc.* 253, 198–206.
- Schwarzenberg-Czerny, A., 1996. Fast and statistically optimal period search in uneven sampled observations. *Astrophys. J.* 460, L107–110.
- Stellingwerf, R.F., 1978. Period determination using phase dispersion minimization. *Astrophys. J.* 224, 953–960.
- Surdej, A., Surdej, J., 1978. Asteroid light curves simulated by the rotation of a three-axis ellipsoid model. *Icarus* 37, 133–141.
- Thomas, P.C. et al., 2007. The shape, topography and geology of Tempel 1 from *Deep Impact* observations. *Icarus* 187, 4–15.
- Vincent, J.-B., Boehnhardt, H., Lara, L.M., 2010. A numerical model of cometary dust structures. Application to Comet 9P/Tempel 1. *Astron. Astrophys.* 512, A60.
- Yeomans, D.K., Chodas, P.W., Sitariski, G., Szutowitz, S., Królikoska, M., 2004a. Cometary orbit determination and non-gravitational forces. In: Festou, M.C., Keller, H.U., Weaver, H.A. (Eds.), *Comets II*. University of Arizona Press, Tucson, pp. 137–151.
- Yeomans, D.K., Giorgini, J.D., Chesley, S.R., 2004b. The history and dynamics of Comet 9P/Tempel 1. *Space Sci. Rev.* 117, 123–135.